ACCSCIENCE PUBLISHING

International Journal of Bioprinting

REVIEW ARTICLE

Three-dimensional printing-based solutions for osteochondral regeneration: Tailoring strategies to region-specific requirements

Maoying Yang[1], Xinyue Tang[1], Yurui Tian[1], Yue Liao[1], Linyi Zhu[2]*, and Haozhe Chen[1,2]*

[1]State Key Laboratory of Oral Diseases & National Center for Stomatology & National Clinical Research Center for Oral Diseases, West China Hospital of Stomatology, Sichuan University, Chengdu 610041, Sichuan, China

[2]Centre for Osteoarthritis Pathogenesis Versus Arthritis, Kennedy Institute of Rheumatology, University of Oxford, OX37FY, Oxford, United Kingdom

Abstract

Tissue engineering (TE) holds significant potential for repairing osteochondral (OC) defects caused by trauma and degenerative diseases. However, the structural and functional heterogeneity between cartilage and bone imposes distinct requirements for regenerative outcomes, while stable integration of the OC interface remains a critical clinical hurdle. Three-dimensional (3D) printing technology, leveraging the advantages of personalized manufacturing and precise structural control, systematically optimizes the synergistic application of core TE elements (cells, growth factors, and scaffolds) during fabrication, offering advanced solutions for OC TE. By mimicking the biomechanics and the physiological regulatory mechanisms of native joints, 3D printing facilitates appropriate microenvironments across material, structural, and mechanical levels. Endowed with outstanding reasoning and predictive advantages, artificial intelligence (AI) has greatly advanced the development of 3D printing. In OC TE, AI exhibits promising applications throughout the 3D printing workflow, including printing process parameter regulation, ink evaluation, and scaffold design optimization. This paper systematically reviews OC TE's general and region-specific requirements, followed by 3D printing's innovative solutions and AI-assisted breakthroughs. Finally, we discuss the limitations and prospects of this interdisciplinary integration of 3D printing and AI in OC TE.

Keywords: Osteochondral regeneration; Tissue engineering; Three-dimensional printing; Artificial intelligence; Machine learning

***Corresponding authors:**
Haozhe Chen
(hz_chen@scu.edu.cn)
Linyi Zhu
(linyi.zhu@kennedy.ox.ac.uk)

Citation: Yang M, Tang X, Tian Y, Liao Y, Zhu L, Chen H. Three-dimensional printing-based solutions for osteochondral regeneration: Tailoring strategies to region-specific requirements. *Int J Bioprint*. 2026:12(2):025490507. doi: 10.36922/IJB025490507

Received: December 2, 2025

1st revised: December 29, 2025

2nd revised: January 13, 2026

Accepted: January 19, 2026

Published online: February 13, 2026

1. Introduction

As a connecting structure between bones, joints perform vital biomechanical functions by enabling lubrication and mediating the transfer and distribution of mechanical loads, thereby ensuring the proper locomotion of the human body.[1] However, trauma or degenerative diseases often result in osteochondral (OC) defects.[2] Without timely treatment, most patients will develop secondary osteoarthritis (OA), leading to progressive joint degradation.[3] Avascular cartilage lacks reparative capacity, while abnormal stress and inflammatory environments impair vascularized bone's reparative

potential, resulting in poor mineralization, fibrosis, and enhanced angiogenesis.[1,3] Currently, total joint arthroplasty is the primary clinical management option for joints with severe impairment.[4] In clinical practice, challenges like infection, post-implant aseptic loosening, and bone resorption undermine the prosthesis's long-term stability *in vivo*.[5] Moreover, revision surgery carries high costs, greater technical complexity, and an elevated risk of postoperative complications, such as infection and ectopic bone formation.[6] Accordingly, there is a critical need for advanced approaches for OC defect repair.

Tissue engineering (TE) integrates scaffolds, cells, and growth factors (GFs) to transition from tissue repair to regeneration, offering new possibilities for treating joint injuries.[7] In contrast to prostheses, TE constructs create bioactive tissues that engage with the implantation site, facilitating adaptive functional reconstruction and ensuring robust biological integration, leading to enhanced long-term stability.[5] OC TE has evolved with a focus on three essential components. Specifically, scaffolds, which serves as a GF delivery platform and cell-supporting matrices, play a crucial role. They not only temporarily fulfill the biomechanical functions of tissues but also create a three-dimensional (3D) microenvironment mimicking natural biochemical and mechanical cues to regulate cellular behavior and facilitate tissue regeneration.[8,9]

Both cartilage and bone in native joints exhibit complex hierarchical and anisotropic structures with mechanical gradient transitions at their interface, making the mimicry of this structural and functional system a primary concern in TE.[4,10] Conventional scaffold fabrication techniques, however, offer a generalized representation of tissues, failing to capture the intricate distribution of components and structures within them.[11] Consequently, random cell seeding and limited inductive effects impede the structural assembly of new tissues, hampering functional tissue formation.[8,12] 3D printing technology, which allows for precise control over product surface and internal structures, has shown significant advantages in scaffold construction for TE.[10] Based on the anatomical and histological understanding of OC tissue, 3D printing seeks to replicate the mechanical properties and biological functions of native joints through material system design, bioactive component distribution, and multi-scale structure construction, effectively enhancing interactions among cells, GFs, and scaffolds and facilitating comprehensive regulation of the regeneration process.[4,13]

Owing to its automated and digital nature, artificial intelligence (AI) demonstrates high efficiency in information extraction, enabling the rapid analysis and integration of large data volumes.[14,15] The utilization of AI has transformed conventional decision-making methods from experience-driven to data-driven approaches, effectively reducing time and resource expenditures resulting from trial-and-error processes.[16] Since 3D printing also depends on digitization for managing manufacturing processes, it inherently aligns with AI-assisted applications, making the integration of AI with 3D printing one of the primary development directions.[17] In the production of TE scaffolds, the application of 3D printing is often constrained by materials and processes, typically relying on empirical testing and refinement.[14,18] In contrast, AI can process extensive datasets through various algorithms, particularly machine learning (ML), which reduces reliance on manually specified rules and presets used in classical AI.[19] With its data-driven autonomous learning and pattern recognition capabilities, ML adapts dynamically to complex patterns and offers advantages in predicting outcomes based on multiple integrated parameters.[20] By integrating the automated control systems of classical AI with the reasoning and predictive capabilities of ML, AI has shown promising application prospects throughout the entire 3D printing workflow, including the control of printing parameters, the printability and biocompatibility of inks, and the structural design of scaffolds.[21]

The integration of 3D printing and OC TE has evolved into a thriving research focus in recent years, with over 400 research articles published during 2020–2025. Existing review papers in this area have generally focused on the structural and compositional heterogeneity between bone and cartilage, while highlighting advanced strategies for achieving OC integrated regeneration.[8,22,23] Yet, the regeneration of the temporomandibular joint (TMJ) condylar fibrocartilage, a tissue with unique articular specificity, has not received sufficient attention or systematic organization. Accordingly, this study presents a comprehensive overview of various tissue types in articular OC tissue, and places special emphasis on the unique properties of TMJ condylar fibrocartilage (Figure 1). Additionally, although current reviews have outlined the application framework of 3D printing in OC regeneration, including printing process selection and ink development, their discussions are largely limited to technical collation and lack targeted solutions tailored to specific tissue regeneration needs.[12,24] To address this limitation, this review integrates interdisciplinary literature resources and incorporates the latest research findings from the past two years (2024-2025), which, guided by the demands of OC regeneration, further discusses the targeted solutions and frontier advances of 3D printing in terms of technology, materials, and scaffold design. In particular, we focus on the potential of AI, a new driving force for development across

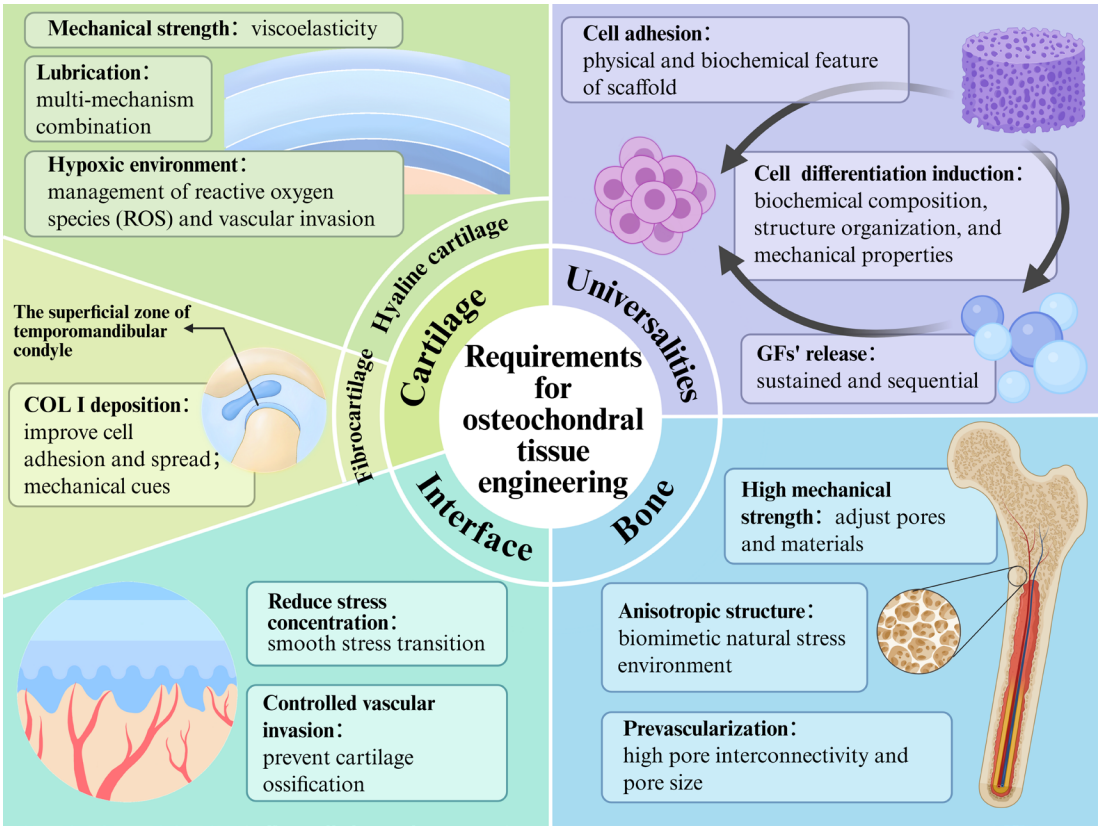

Figure 1. General and region-specific requirements for osteochondral tissue engineering.
Abbreviation: GF: Growth factor

various fields, in OC regeneration when combined with 3D printing. This review clarifies the application prospects and frontier advances of 3D printing–AI integration in this field, discusses the key pathways and bottlenecks in the clinical translation of these advanced concepts and achievements, and aims to provide targeted references for the combined application of these two technologies in OC TE, thus compensating for the limitation of existing reviews, which lack specific focus and practical guidance on AI applications in this domain.

2. Requirements for osteochondral tissue engineering

2.1. General requirements

The successful regeneration of OC tissue imposes general requirements on TE. Among these, the interaction between cells and scaffolds is the most critical factor.[5] In TE, the effective seeding and stable differentiation of seeded cells are fundamental to the regeneration process and are primarily influenced by the physical and biochemical properties of scaffolds and co-regulated by GFs and scaffolds.[1] Effective cell adhesion necessitates the rapid formation of filopodia, which establishes stable adhesion and initiates extracellular matrix (ECM) synthesis.[25,26] Among physical factors, cells require scaffolds with larger internal pore size, porosity, and pore interconnectivity to offer adequate surface area for scaffold interaction and channels for substance transport.[12] Biochemical factors, based on receptor-ligand interactions between scaffolds and cells, require scaffolds to offer stable, controllable adhesion sites for cells through surface components of OC ECM, thereby enhancing cell retention.[9] Expanding upon cell adhesion, scaffolds necessitate further refinement to convey signals mirroring normal developmental processes and morphogenesis, given the pluripotent differentiation potential of stem cells and the challenge of somatic cell dedifferentiation.[13] Researchers have confirmed that scaffold composition, stiffness, stress environment, and surface topography significantly influence gene expression by observing the differentiation trajectory of stem cells.[25,27] Moreover, a deeper understanding of histogenesis highlights the need to mimic native tissues' biochemical composition, structure, organization, and mechanical properties in scaffold design, ensuring scaffolds' long-term *in vivo* stability and improving TE outcomes.[28] Additionally, scaffolds must

exhibit exceptional biocompatibility and biodegradability to avoid a prolonged presence that could trigger an immune response to foreign substances.[29,30] Notably, as a temporary mechanical structure, the OC scaffold should degrade gradually, only after the regenerative tissue has matured to ensure stable and comprehensive support and regulation for the new tissue while mitigating the adverse effects associated with the residual presence of inert materials.[31,32]

Growth factors regulate cell growth, migration, differentiation, and proliferation, serving as essential tools for inducing cell differentiation.[2] While GFs can be endogenously secreted by the body and seeded cells, exogenous supplementation remains necessary to improve the efficiency and quality of TE.[5] Due to their diffusion and hydrolysis *in vivo*, GFs have a short half-life and typically need to be loaded onto scaffolds at supra-physiological concentrations.[1] Frequently utilized GFs in OC TE, including bone morphogenetic protein-2 (BMP-2), transforming growth factor-beta 1 (TGF-β1), and vascular endothelial growth factor (VEGF), are present in serum at low (pg/mL) levels but typically require higher (mg/mL) concentrations for effective dosing in TE, representing a disparity of approximately 5–9 orders of magnitude.[33] Beyond cost considerations, without appropriate delivery strategies to prevent the burst release of these high-concentration GFs, side effects such as abnormal tissue formation, inflammatory complications, and increased cancer risk may occur.[1] Meanwhile, during regeneration, different tissues develop in a certain sequence, and multiple GFs need to regulate cell behavior at different stages by mimicking physiological histogenesis processes.[29] Therefore, to fully exert the therapeutic effects of GFs and avoid side effects, it is necessary to customize GF combinations according to the respective developmental processes of native tissue, and improve GF delivery methods through combined scaffold design to achieve long-term, stable, and sequential release, thereby realizing comprehensive spatiotemporal management of GFs.[33,34]

2.2. Specific requirements for cartilage tissue engineering

The average thickness of articular cartilage (AC) in various human regions ranges from 1 to 4 mm.[35,36] It primarily consists of collagens (COLs) (10–30%), proteoglycans (PGs) (3–10%), and a substantial amount of water (60–80%).[37] Based on the heterogeneity of cellular and ECM components, AC can be categorized into four distinct zones: the superficial zone (SZ), the intermediate zone (MZ), the deep zone (DZ), and the calcified cartilage zone (CCZ).[35] Each of these layers performs unique mechanical functions, presenting challenges for cartilage TE.[38] Most AC is classified as hyaline cartilage (HAC), predominantly composed of type II collagen (COLII). In contrast, the condylar cartilage of the TMJ contains a fibrocartilaginous surface that is primarily composed of type I collagen (COLI).[11,39] This section will specifically address the unique characteristics of this fibrocartilage component.

2.2.1. Hyaline cartilage

The development of HAC originates from mesenchymal stem cells (MSCs) in the mesoderm.[36] Initially, MSCs aggregate spontaneously from a dispersed state to form dense cell clusters, a phenomenon referred to as mesenchymal condensation.[40] This process promotes the chondrogenic differentiation of MSCs through both direct cell–cell interactions and paracrine signaling, while simultaneously establishing a hypotonic microenvironment.[41] During the early weeks of embryonic development, MSCs undergo extensive proliferation and differentiate into chondroprogenitor cells, which subsequently mature into permanent chondrocytes and proliferative chondrocytes.[40] Permanent chondrocytes maintain low proliferative activity and secrete matrix to form HAC, whereas proliferative chondrocytes constitute the growth plate, serving as the basis for endochondral ossification.[38] Cartilage undergoes a maturation process from the embryonic stage to adulthood, during which mechanical stimulation shapes chondrocyte secretory activity and COL organization, gradually transforming the tissue from a uniform structure into a well-defined, four-layered architecture.[36]

The SZ, accounting for approximately 10–20% of the thickness of HAC, contains the lowest amount of PGs and the highest water content, with COL fibers densely arranged parallel to the articular surface to enhance the cartilage's tensile strength and resist shear stress.[23] SZ also acts as a fluid barrier, reducing surface friction via interstitial fluid pressure and bearing over 95% of the external load on the cartilage.[42] Meanwhile, as the primary region for joint lubrication, SZ has a boundary lubrication layer composed of hyaluronic acid (HA), lubricin, phospholipids, and aggrecan.[43] This layer serves as HAC's core lubrication mechanism under high pressure, contributing to the joint's low friction coefficient (0.001–0.3).[44] MZ is the thickest layer in HAC, with loose COLs inclined or randomly arranged relative to the joint surface, capable of resisting compressive force and providing the highest shear strength.[38] With the highest PGs content but the lowest COLs and water content, DZ contains large-diameter COL bundles arranged perpendicularly to the subchondral bone plate (SBP) in a radial pattern, giving it the highest compressive strength.[23] As a natural transition between OC tissue, CCZ is a dense structure with hydroxyapatite (HAP) accounting for 65.09 ± 2.31% of its dry weight.[45]

It connects cartilage and bone at both ends via DZ COLs, forming the tidemark and the cement line, respectively, at two interfaces.[3,36] The uncalcified zone of HAC exhibits a porous structure, with the average pore size of the three layers being 2.5–6.5 nm.[8] As for CCZ, it has an average pore size of 10.71 ± 6.45 nm but a porosity of only 1.6%.[45] This structure results in extremely low permeability throughout the entire cartilage, further establishing the mechanical function of the cartilage.[40,42] Moreover, it forms a hypoxic environment within the cartilage, which is beneficial for maintaining the chondrocyte phenotype and inhibiting catabolism and fibrosis.[37]

The essential requirements for HAC scaffolds can be summarized in three key aspects: mechanical strength, lubrication, and the provision of a hypoxic environment. The mechanical strength of HAC is defined by a compressive strength of 0.08–2 MPa[40], a tensile strength of 5–20 MPa[46], and a shear modulus of 0.07–1 MPa.[47] Constructing a scaffold with adequate mechanical strength is essential for maintaining structural stability under loading, delivering appropriate mechanical cues to resident cells, and providing a foundation for the subsequent remodeling of the zonal organization.[36,40] As lubrication is a key function of cartilage, replicating its high water content and reconstructing an effective boundary lubrication layer are essential for minimizing friction during joint motion and preserving overall tissue integrity.[42,48] Hypoxic conditions are a key factor in regulating chondrocyte phenotype.[7] In TE, although hypoxic tension generally enhances MSC proliferation and promotes chondrogenic differentiation in monolayer cultures, its beneficial effects on chondrogenic induction in 3D culture systems have not yet been conclusively verified.[49,50] It is well established that OA disturbs the native hypoxic environment of cartilage, leading to excessive production of reactive oxygen species (ROS) that damage chondrocyte DNA and impair ECM synthesis. Therefore, effective management of ROS is one of the critical requirements for a successful cartilage TE.[7,37]

2.2.2. Fibrocartilage of the temporomandibular joint condyle

As the only AC composed of fibrocartilage, the TMJ condylar cartilage utilizes its unique superficial fibrocartilage layer to withstand the repetitive and complex mechanical loading of the TMJ throughout life, including protrusion, retraction, lateral movement, mouth opening, and closing.[39] Researchers have reached a consensus that its excellent energy dissipation function is highly associated with the fibrocartilage component.[51]

Condylar cartilage is classified as a secondary cartilage, derived from the ectoderm.[41,52] After MSCs beneath the mandibular periosteum proliferate into secondary cartilage anlagen, the superficial periosteum develops into fibrocartilage, while the anlagen differentiate into HAC and form the condylar bone via endochondral ossification.[53] Thus, condylar cartilage is distinguished from HAC by its unique SZ composed of fibrocartilage. The thickest SZ of the condylar cartilage contains tightly packed, articular surface-parallel COLI bundles and has fewer PGs and water than HAC, resulting in a denser structure.[38,39] Ruggiero *et al.*[46] demonstrated that the tensile modulus of condylar fibrocartilage is 29 ± 13 MPa, which is significantly higher than that of HAC, enabling it to better adapt to the frequent movements of the TMJ. The connection between the SZ and the MZ of condylar cartilage is also mediated by COLI.[38] The structure and function of the remaining layers are similar to those of HAC but with slight differences. According to the zone-specific testing by Gologorsky *et al.*[54], the SZ and DZ of the condylar cartilage exhibit the highest compliance, while the MZ and CCZ primarily resist compressive stress.

Given the unique characteristics of condylar cartilage, TE requires specific design strategies to further distinguish between the fibrocartilaginous and HAC.[55] Some research findings can serve as useful references for the design of scaffolds. For example, Xia *et al.*[25] found that membranes with larger nanopores (200 nm) facilitated increased COLI secretion by promoting cell spreading, nuclear elongation, and cytoskeletal stretching, all of which were reflected in a flattened cellular phenotype. Daly *et al.*[53] compared the chondrogenic induction capacities of several materials and found that alginate and agarose—devoid of natural cell-binding motifs and possessing low stiffness—support HAC formation by maintaining cells in a rounded morphology. In contrast, gelatin methacryloyl (GelMA), which facilitates cell spreading and exhibits higher stiffness, exhibits greater potential for fibrocartilage formation. Furthermore, Wang *et al.*[56] observed that applying excessive mechanical force can augment fibrocartilage formation via mechanosensitive ion channels, particularly Piezo1. These findings highlight the critical role of scaffold structure, mechanical stimulation, and material properties in fibrocartilage formation, while also underscoring the importance of cell morphology (rounded/flattened/spindle-shaped) and migration levels as indicators of chondrogenic differentiation direction.[25,39,57]

2.3. Specific requirements for bone tissue engineering

Bone is composed of ~65% HAP, ~22.5% COLI, along with some lipids and water.[58] HAP provides stiffness, COLs confer toughness, while lipids and water reduce stress via lubrication and interstitial pressurization, thereby

collectively endowing bone with superior biomechanical performance.[59] Bone can be categorized into cancellous bone and cortical bone based on its microstructure. Cancellous bone, located internally, features a trabecular network with a trabecular thickness of 0.1–0.2 mm, pore sizes around 300–500 μm, and a high porosity of 50–95%.[60,61] Despite its relatively low mechanical strength (compressive strength: 0.1–16 MPa), the porous structure of cancellous bone dissipates energy under loading and provides space for the nerves, blood vessels, and bone marrow it contains.[12,59] The natural structure of cancellous bone fully meets the basic requirements of scaffolds throughout the entire process from cell adhesion to tissue regeneration.[61] However, while previous studies have generally described cancellous bone as an isotropic tissue, technological advancements have revealed its heterogeneous and directional characteristics, including pore size as well as trabecular thickness and orientation, which adapt to the stress patterns of different sites.[62,63] Conventional isotropically designed porous scaffolds fail to recapitulate such irregular structures, impeding the provision of stable mechanical support and comprehensive microenvironmental cues.[60]

The external cortical bone comprises mineralized fibrils organized into lamellae.[63] These lamellae are further organized in concentric circles around the central blood vessel, forming the Haversian system, the basic unit of cortical bone.[64] The varying orientations of fibrils within lamellae impart anisotropy to the tissue.[58,60] With a dense structure (porosity: 5–10%), cortical bone exhibits a compressive strength of ~180 MPa and fracture toughness of 2–7 kJ/m^2, functioning as the primary load-bearing component.[12,65,66] Cortical bone has a broad range of pore size, classified into three levels: macropores (20–200 μm) from vascular channels, mesopores (200 nm–15 μm) from lacunae and canaliculi, and micropores (<100 nm) between HAP crystals and COL fibrils, with a natural pore gradient that increases in size toward cancellous bone that enhances stress distribution and mass transport.[58,67,68] Achieving high mechanical strength in cortical bone scaffolds is crucial, but it can hinder porosity and pore size, consequently affecting cell adhesion.[25] As balancing these properties constitutes a challenge in cortical bone TE, mimicking the intricate porous hierarchy of natural cortical bone presents a viable approach, which imposes demands on manufacturing techniques.

The SBP separates CCZ from cancellous bone. It acts as a transitional structure with the pore size of 39.1 ± 26.17 nm and the porosity of 9.7%, with vessels extending from cancellous bone into the CCZ.[3,69] SBP enables smooth stress transmission within OC tissue, while providing a pathway for material exchange on the bony side to support the hypotonic cartilage.[8,29,70] Existing OC scaffolds do not specifically address SBP regeneration; instead, they are usually integrated with the underlying cancellous bone or the CCZ.[4,32]

The structural features of each component impose distinct requirements on the scaffold, and successful bone regeneration also relies on a fundamental basis. Most articular bones form through endochondral ossification.[12] This process starts with the proliferation and hypertrophy of chondrocytes around the growth plate in cartilage, which induces matrix mineralization to form the primary ossification center.[38] Subsequently, stimulated by VEGF, type H vessels invade the mineralized cartilage, facilitating the recruitment of osteoblasts and osteoclasts for bone formation and remodeling.[40,65] Concurrently, vessels serve as conduits for material metabolism and mechanical transduction, while their endothelial cells exhibit high levels of hypoxia-inducible factor-1α to enhance osteogenesis.[71] In bone TE, insufficient osteogenic induction and tissue center ischemic necrosis are two primary causes of failure resulting from poor vascularization.[68] Reconstructing the vascular network is essential for reestablishing bone metabolic function and ensuring the enduring viability of regenerated tissue. Based on the histological and functional characteristics of cartilage and bone, the similarities and distinctions in their scaffold requirements were compared and summarized in Table 1.

2.4. Specific requirements for osteochondral interfaces in tissue engineering

Cartilage and bone are anchored by the comb-like cement line.[3] The stable integration depends not only on mechanical interlocking at the interface, but also on the compositional and structural gradient transitions formed between CCZ and SBP.[70] From uncalcified cartilage to CCZ, the content of COLII and water, as well as porosity, decrease gradually, while tissue stiffness increases; from CCZ to SBP, HAP content further rises, COLII transitions to COLI, and vessels emerge.[23,69] Additionally, the development and maturation of cartilage and bone involve progressive regional differentiation, enabling tight bonding between various layers through COLs.[36,45] This smooth transition aligns closely with the sophisticated graded shock-absorption systems in engineering (e.g., building, bridge, and tunnel construction), which achieve the gradual absorption of vibration energy and uniform transmission of stress, thus guaranteeing stable structural integration.[72] The primary goal of scaffold interface design is to mimic such structural and mechanical transitions, facilitating appropriate force transmission, absorption, and dissipation.[2,4]

Table 1. Similarities and distinctions between cartilage and bone scaffold requirements in tissue engineering

Parameters	Cartilage	Bone
Similarities	Mechanical strength requirements; porous structure; anisotropy; general requirements include cell adhesion, phenotype regulation, biosafety, and biodegradability	
Distinctions	High water content; mineralization inhibition; viscoelasticity; lubrication capability; surface-to-deep layered structure; small pore size; restriction of vascular invasion; hypoxic microenvironment	Low water content; mineralization promotion; high compressive strength; external-to-internal layered structure; large pore size; prevascularization
References	37,39,40,44,45	3,40,58,64,69

Beyond mechanical functions, the OC interface also serves as a pathway and barrier for crosstalk between the two tissues. A small number of vessels from cancellous bone extend into the CCZ and transmit mineralization signals for the CCZ via oxygen. However, the excessive invasion of the vessels is observed in OA, leading to abnormal cartilage calcification, fibrosis, and intra-articular ossification, which impairs joint stability.[23,73] Consequently, it is essential to consider the region-specific patterning of vascularization in OC reconstruction to preserve the hypoxic environment of cartilage.[7,11]

3. Three-dimensional printing-based solutions for general requirements

3.1. Three-dimensional printing technologies

Three-dimensional printing, also referred to as additive manufacturing (AM), enables the precise fabrication of highly customized products through the layer-by-layer deposition of materials.[31] By converting the 3D modeling of the product into two-dimensional slicing, 3D printing can attain high-precision replication of both the internal structure and external contour of the model through thinner layers and higher accuracy.[10,62] Compared to traditional scaffold fabrication methods, such as phase separation, foaming, microsphere sintering, and electrospinning, this approach more effectively mimics the anisotropic and complex OC tissue.[18] Particularly, it allows for the incorporation of multiple materials to promote the integration of the OC interface via a unified design.[2] Furthermore, the integration of bioactive components such as cells, GFs, and decellularized ECM (dECM) has advanced 3D printing into the realm of 3D bioprinting, thereby achieving a more thorough optimization of TE.[64,73] Traditional 3D printing is categorized into four types based on the printing mechanism: inkjet-based 3D printing (IJP), extrusion-based 3D printing (EBP), vat photopolymerization-based 3D printing (VPP), and laser-assisted 3D printing.[55,74] This section will introduce the mechanisms and suitable materials for each of these printing technologies, discuss their pros and cons in the fabrication of OC scaffolds, and evaluate their ability to preserve bioactivity, particularly cell viability, during 3D bioprinting (Figure 2). Furthermore, their clinical translation potential in OC TE is comprehensively summarized in Table 2.

3.1.1. Inkjet-based three-dimensional printing

Inkjet-based 3D printing is a widely adopted printing technology derived from traditional two-dimensional inkjet printing, but the limited mechanical strength of the resulting scaffolds restricts its use to niche applications in cartilage scaffold fabrication.[74] Its process mainly involves two steps: inkjetting and solidification (via light or temperature).[75] The prevalent droplet driving mechanisms are thermally driven and piezoelectrically driven.[8]

Thermal IJP (TIJ) functions by rapidly heating the nozzle to over 300 °C within a few microseconds, resulting in the instantaneous vaporization of the ink.[76] The high pressure produced by the expanding bubbles ejects droplets onto the substrate.[77] With up to 600 nozzles and a minimum droplet volume of approximately 10 pL, TIJ facilitates high-speed printing with micrometer-level precision.[78] However, the high-temperature foaming mechanism imposes additional requirements on the vaporizable properties and stability of the ink, thereby restricting material selection.[24] Furthermore, the sizes of nozzles and droplets are relatively fixed and difficult to adjust.[78] Nevertheless, despite the process of heating, the brief exposure to high temperatures minimally affects cell viability, with cell activity retention reaching up to 95% in TIJ-based bioprinting.[55]

Piezoelectric IJP (PIJ) utilizes voltage pulses to deform piezoelectric elements, generating pressure waves inside the nozzle to eject the ink.[76] Compared to TIJ, PIJ offers the advantage of easily adjusting droplet size, achieving a minimum volume of one pL per droplet, thereby enhancing printing resolution.[24] Additionally, since PIJ involves no significant temperature fluctuations, it does not impose constraints on the thermal characteristics of the ink.[79] However, the high-frequency vibration of piezoelectric elements can damage cell membranes and biomolecular structures, limiting PIJ's advancement

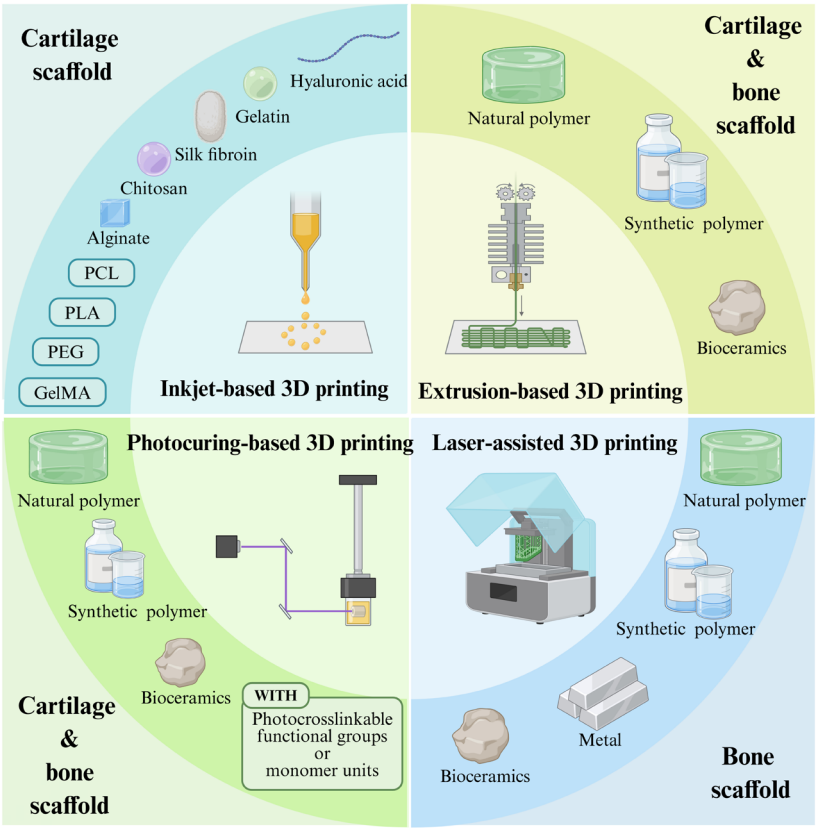

Figure 2. Three-dimensional (3D) printing technologies and compatible materials
Abbreviations: GelMA: Gelatin methacryloyl; PEG: Polyethylene glycol; PCL: Polycaprolactone; PLA: Polylactic acid.

toward bioprinting.[70]

The feature resolution of these two traditional driving methods is often constrained due to the limitations of ink viscosity, surface tension, and component particle size.[76] As a new driving method, electrostatic IJP has optimized the shortcomings of both. By utilizing electrostatic force to overcome surface tension, it can use inks with a wider viscosity range and avoid the impact of heat and instantaneous pressure on bioactive components, achieving nanometer-level precision.[79,80] However, compared with TIJ and PIJ, electrostatic IJP has a higher cost, thus limiting its applications.[78]

3.1.2. Extrusion-based three-dimensional printing

Extrusion-based 3D printing is similar to IJP but can extrude inks continuously across a wide viscosity range (30–6 × 10^7 mPa/s) using mechanical or gas-driven methods, resulting in seamless filaments.[24,81] It is easy to operate and suitable for both bone and cartilage scaffold fabrication.[7,12] EBP-based bioprinting also allows for high cell densities in the bioink, but filament-dragging issues may arise from direct deposition onto non-smooth substrates with complex topographies.[82] Additionally, the shear stress during extrusion results in a cell viability retention rate of 90%.[69,74] In contrast, inks with lower viscosity that require relatively low extrusion pressure facilitate the improvement of cell viability preservation.[77,83] By simultaneously printing support structures and target structures with multiple printheads, low-viscosity inks can obtain temporary mechanical support to ensure printing accuracy.[75,82]

Fused-deposition modeling (FDM) is a widely used method of EBP.[14,68,84] By heating thermoplastic or low-melting-point materials to a molten state (100–300 °C) and extruding them via mechanical drive, FDM can print relatively regular structures with a precision of 60–600 μm.[9,85]

Addressing the high-temperature constraints of FDM and aiming to improve bioink applicability, Xiong *et al.*[86]

developed low-temperature deposition manufacturing (LDM) and applied it to the production of OC scaffolds. Operating within a temperature range of −30 to 0 °C, LDM is particularly suited for preserving the bioactivity of bioinks.[87] Additionally, LDM incorporates phase separation technology, with the solvent being removed through vacuum freeze-drying, which can achieve controllable pore size and pore interconnectivity. This capability allows for the creation of hierarchical porous structures spanning micro to nano scales, rendering it particularly advantageous for bone TE.[31,87] Inks with good fluidity and rapid solidification in the forming chamber, as well as solvents with strong solubility and moderate volatility, are the key factors of achieving high-fidelity structure fabrication via LDM, while simultaneously posing the primary limitations to its development.[67] Moreover, the demand for ink fluidity and the compromised interlayer bonding strength at low temperatures often lead to poor mechanical performance of LDM products.[88] To reconstruct the mechanical functions of bone and cartilage, ongoing optimization of ink formulation and nozzle temperature is necessary.

3.1.3. Vat photopolymerization-based three-dimensional printing

Vat photopolymerization-based 3D printing utilizes optical projection to induce layer-by-layer polymerization and solidification of liquid photosensitive resins.[12] Without nozzles, it avoids ink clogging and precludes cell viability interference from pressure and shear stress, with cell viability remaining above 85%.[55,89] While it enables the fabrication of both bone and cartilage scaffolds, its application in large-scale bone scaffold fabrication is restricted by the generally inferior mechanical strength.[4,66,77] Based on control systems and light source, VPP is categorized into stereolithography (SLA), digital light processing (DLP), and two-photon polymerization (TPP).[24]

As the most classic VPP method, SLA triggers polymerization point-by-point in the XY direction according to a predefined pattern using ultraviolet or visible laser beams.[26] It enables rapid fabrication of high-precision products with a resolution of up to 10 μm.[66] Notably, SLA can also achieve high-precision control over the internal structure of products, capable of manufacturing gradient porosity bone scaffolds with pore sizes ranging from 500 μm to 3 mm at a resolution of 60 μm.[90] DLP crosslinks entire resin layers simultaneously using digital micromirror devices, further optimizing the fabrication time and precision of SLA.[4,91] Additionally, DLP offers advantages in printing complex and overhanging structures, allowing customization of pore shape and interconnectivity, with lower equipment costs and energy consumption.[34,64] Unlike SLA and DLP, which achieve solidification through single-photon excitation of individual molecules, TPP employs femtosecond pulsed lasers (λ = 600–1,000 nm) to enable a single molecule to absorb two photons simultaneously in a submicron volume, thereby excited to a higher energy state.[24] This approach enables fabrication with enhanced penetration and superior resolution of 100 nm.[92] However, the application of TPP is limited by its low processing efficiency and high laser power requirements.

One of the key challenges hindering the broader adoption of VPP is material limitations. VPP inks mainly consist of photosensitive resin matrices (epoxy resins, acrylates, urethane acrylates) and photoinitiators.[4,8] For OC scaffolds, metals or bioceramics are usually added as fillers to enhance mechanical strength, which leads to filler dispersion issues. Uneven filler distribution can form more scattering centers, resulting in local over-curing and reduced precision.[93] Moreover, low-viscosity inks are preferred in VPP for their shorter curing time, reduced surface tension, and faster, more uniform thin-film formation, thereby improving product precision. A notable drawback, however, is that low-viscosity inks are more prone to cell sedimentation, resulting in uneven cell distribution.[24] Furthermore, polymerization processes are generally accompanied by shrinkage, which affects the accuracy of products, thus requiring additional compensation measures.[66] In addition, although VPP-based bioprinting reduces mechanical harm to cells, cell viability may still be compromised by photoinitiators, residual monomers, and excessive laser power. Further optimization is needed to utilize biocompatible materials and shorten curing time, thereby adapting to bioink applications.[12,77,92]

3.1.4. Laser-assisted three-dimensional printing

Laser-assisted 3D printing mainly includes powder bed fusion (PBF) and laser-induced forward transfer (LIFT). It uses lasers as the energy source and does not require a nozzle.[94] However, unlike VPP, it leverages the thermal effects of higher-energy lasers to sinter, melt materials, or generate mechanical driving forces.[95] Its products possess excellent mechanical strength, making them highly suitable for bone scaffold fabrication.[61,62]

Powder bed fusion employs lasers to selectively fuse preheated thin layers of micrometer-scale powder on the substrate, enabling the construction of objects with complex shapes and porous characteristics without the need for printing support structures.[94] Selective laser melting (SLM) and selective laser sintering (SLS) are the most widely used PBF methods.[24] By directly melting metal or alloy powder into a liquid state with a high-power laser, followed by rapid cooling and solidification,

Table 2. Advantages and disadvantages of three-dimensional printing technologies in clinical translation for osteochondral tissue engineering

Three-dimensional printing technology	Advantage	Disadvantage	References
Inkjet-based three-dimensional printing	High precision; high throughput; high cell viability retention; moderate cost	Narrow ink viscosity window; generally inferior mechanical strength of scaffolds	55,75,76,78
Extrusion-based three-dimensional printing	High throughput; superior material compatibility; wide ink viscosity window low cost	Low precision; low cell viability retention; supporting structures required	14,81,85
Vat photopolymerization-based three-dimensional printing	High precision; superior in porous structure fabrication	Limited printable size; limited mechanical strength of scaffolds; photocurable resins requirement; low cell viability retention; polymerization shrinkage; filler dispersion; high cost	8,24,55,92,93
Laser-assisted three-dimensional printing	High precision; generally superior mechanical strength of scaffolds; no supporting structures required	Limited material adaptability; low cell viability retention; high cost	24,61,94,95

SLM can fabricate dense structures. The products exhibit excellent mechanical properties with a precision of up to 100 μm.[61] Moreover, the rough surface of SLM products due to adhesion of incompletely melted powder has also been proven to enhance cell adhesion.[96] In contrast, SLS uses lower laser intensity, only melting the powder surface to induce sintering. The products of SLS are porous, with lower precision and strength compared to SLM.[11,62] Nevertheless, compared to SLM, SLS is compatible with a variety of metals, ceramics, and thermoplastic polymers, and consumes less energy.[97]

Due to its reliance on high temperatures, PBF is not suitable for bioactive materials. Laser-assisted 3D bioprinting is mainly realized through LIFT. LIFT uses lasers to vaporize the ink at the donor ribbon, forming high pressure to eject it onto the receiving substrate.[95,98] This is a method similar to TIJ, but since no nozzle is required, LIFT-based bioprinting is not limited by ink viscosity and demonstrates better cell viability retention (>95%).[99] Additionally, it can print large-volume (100–300 μm) stem cell spheroids, enabling high-density and high-throughput cell-laden 3D bioprinting.[100]

3.2. Materials for three-dimensional-printed osteochondral scaffolds

Common scaffold materials in OC TE include four categories: natural polymers, synthetic polymers, metals, and bioceramics.[99] Overall, natural polymers exhibit superior biocompatibility, bioactivity, and biodegradability, but have poor mechanical strength, rapid degradation rates, and potential immunogenicity.[74,77,81] Synthetic polymers typically possess higher mechanical strength and processability, with slow degradation, yet they lack bioactivity.[69,79] Metals offer high strength, and most metal ions have osteoinductive properties, but they are prone to stress shielding and difficult to degrade.[83,94] Bioceramics, on the other hand, have excellent biocompatibility, bioactivity, and mechanical strength; they release calcium ions, phosphate ions, and silica, which exhibit osteoinductivity, and their inherent porous structure is suitable for tissue ingrowth. However, bioceramics are relatively brittle and have poor processability.[61,86] Table 3 lists the advantages,

Table 3. Advantages, disadvantages, and appropriate three-dimensional printing technologies for various materials applied in osteochondral tissue engineering

Type/material		Advantage	Disadvantage	3D printing technology	Ref.
Natural polymer	COLs	Biocompatibility; bio-adhesiveness; bioactivity; self-renewable	Poor mechanical strength; immunogenic; slow gelation rate; poor shape fidelity	FDM; LDM; LIFT	4,7,70,74,77
	HA	Bio-adhesiveness; high porosity; lubrication; maintain hydration level; highly diffusible and absorbable; enhance chondrogenic differentiation; rapid gelation rate	Low stability; poor mechanical strength; lack of bio-adhesiveness; high viscosity; poor shape fidelity	IJP; FDM; SLA; DLP; LIFT	82

(*Cont'd...*)

Table 3. *Continued*

Type/material		Advantage	Disadvantage	3D printing technology	Ref.
Natural polymer	Gelatin	Biocompatibility; low immunogenic; modifiable; rapid gelation;	Poor mechanical strength; fast degradation rate; high brittleness; low chemical stability;	IJP; FDM; LDM; SLA; DLP; TPP; LIFT	10,30,70,77,95
	Alginate	Biocompatibility; biodegradability; chemical stability; modifiable	Poor shape fidelity; lack of bio-adhesiveness; low viscosity;	IJP; FDM; LDM; SLA; LIFT	69,70
	Chitosan	Biocompatibility; biodegradability; renewability; antimicrobial; bio-adhesiveness;	Poor mechanical strength; poor shape fidelity; low thermal stability; rapidly dissolves under pH 6.5	IJP; FDM; LDM; SLA; DLP; TPP	70,81
	Cellulose	Biocompatibility; chemical stability; insolubility; high porosity; high elastic	Low biodegradability; poor mechanical strength; unable to melt	FDM; SLA; DLP; LIFT	77
	Agarose	Biocompatibility; biodegradability; good mechanical strength; rapid gelation rate; modifiable	Lack of bio-adhesiveness; high viscosity	FDM	101
	Fibronectin	Biocompatibility; biodegradability; controllable mechanic strength;	Poor mechanical strength; high viscosity; fast degradation rate	LIFT	70,99
	Silk fibroin	Biocompatibility; great mechanical strength; controllable biodegradability; osteoinductivity; capable of non-covalent bonds; thermal stability	Lack of bio-adhesiveness; low viscosity; high brittleness;	IJP; FDM; DLP; LIFT	76,82,87
	dECM	Biocompatibility; biodegradability; tissue-specific differentiation-inducing ability	Poor mechanical strength; fast degradation rate;	LDM; SLA;DLP;	48,89
Synthetic polymer	PCL	Biocompatibility; non-toxic biodegradability; good mechanical strength; modifiable; low immunogenicity; thermal stability;	Lack of bio-adhesiveness; hydrophobic;	IJP; FDM; LDM; SLA; DLP; TPP; SLS	11,69,73,75
	Polyvinyl alcohol	Biocompatibility; biodegradability; high mechanical strength; chemical stability;	Lack of bio-adhesiveness; hydrophobic;	FDM; SLA; DLP; SLS;	10
	Polylactic acid	Biocompatibility; non-toxic biodegradability; shape memory effect	Lack of bio-adhesiveness; brittleness; acidic degradation products inhibit osteogenesis	IJP; FDM; SLA; DLP; TPP; SLS; SLM	2,66,84,101
	PEG	Biocompatibility; hydrophilic;	Poor mechanical strength; non-biodegradable; hydration layer resists cell adhesion	IJP; FDM; SLA; DLP; SLS	8,84,91,92
	Polyglycolic acid	Biocompatibility; high mechanical strength; hydrophilic	Lack of bio-adhesiveness; fast degradation rate; acidic degradation products;	FDM; SLS	12
	Poly(lactic-co-glycolic acid)	Biocompatibility; controllable biodegradability; modifiable	Poor mechanical strength; hydrophobic; rapid disintegration; acidic degradation products	FDM; LDM; SLA; DLP; TPP; SLA	29,88
	Polyetheretherketone	Biocompatibility; high mechanical strength; thermal and chemical stability	Non-biodegradable; lack of bio-adhesiveness	FDM; LDM; SLS; SLM	9,67
	GelMA	Biocompatibility; bio-adhesiveness; controllable mechanic strength; enhance chondrogenic differentiation; low immunogenicity; thermal stability; suitable viscosity	Lack of osteoinductivity	IJP; FDM; SLA; DLP; TPP	73,77,79
	Polyurethane	Biocompatibility; biodegradability; regenerativity; hydrophilicity; shape memory effect; high elastic	Lack of bio-adhesiveness and bioactivity	FDM; LDM; SLA; DLP; TPP	55,88

(*Cont'd...*)

Table 3. *Continued*

Type/material		Advantage	Disadvantage	3D printing technology	Ref.
Synthetic polymer	Acrylonitrile butadiene styrene	Biocompatibility; suitable melting point (200°C); chemical stability	Poor biodegradability; hydrophobic	FDM; SLA; DLP	24
	Polypropylene	Biocompatibility; chemical stability	Poor biodegradability; hydrophobic; low rigidity	FDM	24
Metal	Titanium	Biocompatibility; high mechanical strength; rapid osseointegration; low biological toxicity, corrosion resistance	Non-biodegradable; slightly rough surface; high-stress shielding; bioinert	SLS； SLM	10,27,62,96
	Magnesium	Biodegradability; bioactivity; elasticity modulus approximates bone; osteoinductivity; regulates bone metabolism; immune regulation	Rapid corrosion; toxic side effects and H_2 release during degradation;	SLS; SLM	83,94,102
	Tantalum	Biocompatibility; bioactivity; high mechanical strength; osteoinductivity; structural continuity; non-deformability; corrosion resistance	Non-biodegradable	SLS; SLM	61
	Aluminum	High mechanical strength; corrosion resistance	Poor biodegradability	SLS; SLM; LIFT	94
	Copper	Osteoinductivity; broad-spectrum and high-efficiency antibacterial effect; immune regulation	Dose-dependent cytotoxicity; rapid corrosion	SLS; SLM; LIFT	9,98
	Silver	Broad-spectrum and high-efficiency antibacterial effect	Dose-dependent cytotoxicity	SLS; SLM	98
	Zinc	Biocompatibility; biodegradability; osteoconductivity; osteoinductivity; antimicrobial; immune regulation; corrosion resistance	Poor mechanical strength; mild cytotoxicity	SLS; SLM	94
Bioceramics	HAP	Biocompatibility; biodegradability; high porosity; osteoconductivity; osteoinductivity	High brittleness; rapid degradation rate	FDM; SLA; DLP; SLS; SLM; LIFT	69,70,73,90
	Tricalcium phosphate	Biocompatibility; biodegradability; osteoconductivity; osteoinductivity;	Poor mechanical strength	FDM; LDM; SLA; DLP; SLS; SLM	8,10,86
	Bioactive glass	Biocompatibility; controllable biodegradability; osteoconductivity; osteoinductivity; antimicrobial;	High brittleness; poor porosity;	FDM; SLA; DLP; SLS; SLM	8,9,64,95,96
	Calcium sulfate	Biocompatibility; osteoconductivity;	Fast degradation rate	FDM; SLA; DLP; SLS	103
	Zirconia	Biocompatibility; high mechanical strength; osteoinductivity; corrosion resistance;	High brittleness	FDM; SLA; DLP; TPP; SLS; SLM	102

Abbreviations: 3D: Three-dimensional; COLs: Collagens; DLP: Digital light processing; dECM: Decellularized extracellular matrix; FDM: Fused deposition modeling; GelMA: Gelatin methacryloyl; HA: Hyaluronic acid; HAP: Hydroxyapatite; IJP: Inkjet printing; LDM: Liquid deposition modeling; LIFT: Laser-induced forward transfer; PCL: Polycaprolactone; PEG: Polyethylene glycol; SLA: Stereolithography; SLM: Selective laser melting; SLS: Selective laser sintering; TPP: Two-photon polymerization.

disadvantages, and applicable 3D printing technologies of each material in OC TE.

3.3. Three-dimensional printing-based solutions for cells and growth factors

3.3.1. Scaffold-mediated cell adhesion and differentiation induction

Three-dimensional-printed scaffolds can synergistically enhance cell adhesion while delivering various differentiation signals.[62] First, 3D printing allows for highly customized scaffold pore characteristics, particularly excelling in the precise control of pore size, interconnectivity, and distribution.[13,89] Utilizing 3D printing enables the creation of nanoscale pores to replicate a hypoxic setting to induce chondrogenic differentiation, produce scaffolds with 100% pore interconnectivity to tailor channels for bone vascularization, and adjust pore distribution to imitate the natural pore distribution, replicating the physiological pore transition in OC for monolithic formation.[67,91,104,105] By adjusting porosity, distinct mechanical properties can be designed, which in turn provide specific mechanical signal cues for cell differentiation. Li *et al.*[106] developed a microwave fabrication method based on FDM to produce micrometer-scale microfiber networks that mimic the natural ECM, which can provide effective geometric and mechanical signals for cells to induce directed cell migration and osteogenic differentiation. Feng *et al.*[107] demonstrated that scaffolds with oriented channels are more conducive to cell migration and infiltration compared to randomly porous scaffolds, avoiding fibrosis and poor mineralization during regeneration. Ghobadi *et al.*[68] integrated microchannels in three directions into a scaffold by FDM, successfully simulating the bone vascular network to enhance osteogenesis. The ZigZag-Spiral pattern can mimic the inward-outward pore transition and radial channels of natural bone, provide uniform mechanical support, exhibit optimal cell adhesion efficiency, and support uniform differentiation of internal cells. In addition, in the traditional static seeding method, cells cannot be uniformly distributed in the scaffold due to gravity, resulting in excessively high or low local cell density, which is unfavorable for cell secretion and prone to dedifferentiation.[48,87] In contrast, dynamic seeding, whether via centrifugation or perfusion bioreactors, incurs considerable time and equipment expenses.[85] 3D bioprinting offers a more convenient approach for cell seeding. Its application enables the simultaneous implementation of scaffold fabrication and cell seeding, eliminating the time required for cell adhesion.[69,75] It is particularly effective in improving the seeding efficiency of scaffolds with complex structures and achieving precise regulation of cell distribution.[100]

Three-dimensional printing also facilitates the fabrication of scaffolds with complex surface topography.[104] Porous structures not only increase the scaffold surface area but also typically facilitate the formation of rough surfaces, providing additional sites for cell–scaffold interactions and guiding cell migration.[24,55,58] Taking this further, complex substrate topographies can be specifically designed to regulate cell adhesion and achieve directed cell growth; additionally, by adjusting cell contractility, it can influence protein aggregation on the MSCs membrane and subsequently activate various cell signaling pathways.[25,26] Nanoscale surface topographies are reported to enhance cell adhesion and directional migration, while microscale surface configurations impede cell motility but confer a beneficial impact on osteogenic differentiation.[108] Notably, surface curvature exerts a critical regulatory effect on cell differentiation. Scaffolds featuring minimal surface curvature support the maintenance of chondrocytes' rounded phenotype, whereas those with moderate curvature enhance the expression of key osteogenic differentiation factors.[20,96,109] Triply periodic minimal surfaces (TPMS) are the most advanced structures for OC scaffolds, with zero mean curvature and a high specific surface area similar to that of natural bone.[110] Due to their 3D continuity, TPMS can simultaneously regulate both surface and internal structural attributes, including surface roughness, surface curvature, pore size, and pore interconnectivity.[93] Using FDM, Mushtaq *et al.*[111] tested various TPMS lattice structures and identified the advantages of the Gyroid structure in terms of surface roughness and porosity for cell interactions. Yang *et al.*[26] investigated Gyroid-type TPMS with a surface curvature of −2 to ~−6 mm^{-2}, highlighting the critical influence of surface curvature on bone and vascular regeneration.

Furthermore, 3D printing techniques, such as IJP and EBP, can be utilized for post-processing to create intricate surface topographies. Serving as a precise and effective coating approach, 3D printing broadens the utilization of diverse coating materials, facilitating not only the chemical alteration of scaffold surfaces but also the deposition of materials in defined micropatterns.[30,76] Beyond serving as an AM technique, IJP can be combined with wet etching, where etchant inks are employed to facilitate subtractive manufacturing, thereby circumventing the issue of inadequate coating-scaffold adhesion.[111]

3.3.2. Scaffold-mediated sustained and sequential release of growth factors

Growth factors are commonly integrated into scaffolds through noncovalent techniques, such as adsorption, binding to ECM components, and encapsulation.[1] Adsorption is a simple yet highly unstable approach with

no regulatory capacity.[50] Since ECM components such as HA, chondroitin sulfate, and fibronectin naturally contain GF-binding domains, they have been demonstrated to facilitate the sustained release of GFs.[1] However, the nonspecific interactions between GFs and ECM can lead to broad and uncontrollable cellular responses.[112] Among these methods, encapsulation is the primary strategy for sustained GFs release.[1,32] By encapsulating GFs into carriers, such as hydrogel microspheres or nanoparticles, before incorporating them into scaffolds, burst release can be effectively avoided, enabling stable and long-term regulatory effects.[84] 3D bioprinting facilitates the encapsulation of GFs by enabling the direct utilization of GFs and GF-loaded delivery vehicles as ink components for printing. This method allows precise control over their spatial arrangement within the scaffold, leading to the creation of GF gradient systems.[113] There are also attempts to regulate GF release by designing the structure of encapsulation materials via 3D printing. Wang *et al.*[34] reported a specialized GF controlled-release tool: millimeter-scale cylindrical structures with a core-shell architecture fabricated via DLP and photopolymerizable hydrogels. The release kinetics of internal GFs were modulated by adjusting the shell thickness.

Sequential release is usually achieved by altering the GF loading method or materials. GFs targeted for early release are generally directly coated onto the scaffold's surface or encapsulated within fast-degrading materials (mostly natural polymers). In contrast, GFs that exert biological effects in the late stage of tissue regeneration are encapsulated internally via slow-degrading materials (synthetic polymers such as polycaprolactone [PCL] and polylactic acid [PLA]).[33,114] Sequential GF release can also be realized through 3D bioprinting. By varying the VPP curing time, the crosslinking density of the scaffold differs, which enables the regulation of GF release kinetics.[115]

4. Three-dimensional printing-based fabrication of cartilage scaffold

4.1. Hyaline cartilage

4.1.1. Mechanical strength

As a tissue that achieves energy buffering through its high water content structure and viscoelastic mechanical properties, the biomimetic design of HAC scaffolds is mainly realized by hydrogels that possess analogous characteristics.[32,69,116] However, while hydrogels, particularly natural polymer hydrogels, exhibit mechanical and biochemical properties that can induce the secretion of cartilage ECM, their mechanical strength is insufficient to meet the weight-bearing demands of HAC, with most having a compressive modulus only 10% of that of native HAC.[87,117] Increasing crosslinking density within a certain range significantly improves the mechanical strength of hydrogels, while simultaneously reducing their swelling and improving structural stability, shape fidelity, and decreasing degradation rate.[101] Nevertheless, excessive crosslinking can also compromise hydrogel porosity and printability, while impeding cell proliferation and migration.[29,81,92] Given the limitations of hydrogels and the multifunctional demands of scaffolds, researchers in cartilage TE have begun to adopt structural modification and composite formulations for HAC scaffolds.[83] Beyond improving mechanical properties with composite materials, researchers have drawn inspiration from the natural double interpenetrating polymer network (IPN) structure of HAC, which is formed by COLs and PGs.[7,117] This has rendered IPN a prevalent strategy for designing composite hydrogel networks in cartilage TE, which has been successfully combined with 3D printing methods.

Through the synergistic effect of ionic and chemical crosslinking, IPN interweaves multiple independent polymer networks into a composite structure, leading to significant improvements in the system's dispersion, interfacial affinity, and phase stability.[118] With a rigid primary network and a flexible secondary network, double network (DN) hydrogels facilitate the stable combination of diverse materials with different favorable properties in a relatively simple way, satisfying the mechanical and biochemical demands of HAC TE.[7,119] Most DN hydrogels are synthesized via a two-step process: the rigid primary framework of the DN scaffold is often fabricated using 3D printing to provide a precise basic structure; flexible cell-laden hydrogels are then incorporated, leveraging 3D printing's manufacturing benefits while circumventing cell viability concerns during the process (Figure 3A).[120] Notably, the incorporation of photosensitive and thermosensitive materials enables the single-step printing fabrication of DN hydrogels, thereby effectively enhancing the shape fidelity and structural accuracy of the final product.[118] Going a step further, conventional IPNs suffer from weak interfacial interactions and asynchronous deformation under stress due to their exclusive dependence on molecular chain entanglement for network connection.[121] To tackle this issue, the introduction of diverse crosslinking bonds through a dual cross-linking design can reinforce interfacial bonding between networks and improve overall system stability.[122] For example, Gupta *et al.*[121] activated the surface of FDM-printed PLA during post-processing, incorporating dual cross-linking IPN hydrogel with Schiff base bonds and ionic bonds through covalent bonds to create a cartilage scaffold with stable load-bearing capacity, self-healing ability, and excellent biocompatibility. Sasikumar *et al.*[118]

modified mucin with photosensitive groups, combined it with alginate, HA, and chondrocytes to produce a bioink, and utilized photocuring post-biofabrication via EBP-based bioprinting. This approach not only streamlined fabrication into a single printing step but also effectively increased the compressive modulus of the scaffold to the level of natural HAC through dual cross-linking (Figure 3B).

4.1.2. Lubrication

Hydrogel scaffolds can replicate the hydration lubrication characteristic of HAC, thereby providing a lubricating effect; however, relying solely on the hydration lubrication inherent to hydrogels is still inadequate.[123] One primary reason for the compromised lubricating capacity is that most hydrogels demonstrate poor stability under cyclic loading or high mechanical loads, making them susceptible to wear and abnormal swelling.[116,124] Although enhancing mechanical properties can address this stability challenge, the lubricating efficacy remains unable to match that of natural HAC. For instance, despite being classified as ultra-tough gels, DN hydrogels demonstrate inadequate energy dissipation capacity, as they rely almost exclusively on the breakage of the primary network, leading to a relatively high coefficient of friction (CoF; $\mu \approx 10^{-1}$).[125] Since boundary lubrication is the predominant lubrication mechanism for HAC under high interfacial pressure, replicating this lubricating layer is a key challenge in HAC biomimetic design.[43] Currently, the primary approaches focus on incorporating natural boundary lubricants, primarily through microparticle loading or IPN structure refinement.[48]

Incorporating natural boundary lubricants as fillers into hydrogels can create a microreservoir structure that can be squeezed out onto the interface under stress to form a boundary lubricating layer.[116,126] Lin *et al.*[127] demonstrated that incorporating phosphatidylcholine (PC) liposomes into hydrogels yielded a significantly enhanced lubricating effect (CoF as low as 0.01) compared to their use as external lubricants. Similarly, Li *et al.*[128] fabricated porous hydrogels via dialysis (used as a porogen) to load HA, and successfully established a boundary lubricating layer during 3D printing post-processing (Figure 3C). A major limitation, however, is that these lubricating particles are fixed within the hydrogel network and lack the ability to migrate freely in response to stress. Consequently, when the boundary layer is damaged under shear stress, the unstable lubricants cannot be re-exposed until the overlying hydrogel is worn, leading to compromised lubrication stability.[124]

The IPN optimization strategy for introducing a boundary lubricating layer primarily focuses on the design of a third network within DN hydrogels. To balance the mechanical strength and lubricating capacity of DN hydrogels, Kaneko *et al.*[129] pioneered the modification of these materials as early as 2005 by incorporating a weakly crosslinked third network to reduce the CoF. This approach has since been widely adopted by researchers for the construction of HAC scaffolds. The third network is the lubrication-dominant structure and can be formulated with natural boundary lubricants. In the study by Milner *et al.*[130], the integration of a poly(2-methacryloyloxyethyl phosphorylcholine) third network reduced the CoF of DN hydrogels by 47% at a specific velocity via boundary lubrication mechanisms. Ali *et al.*[124] investigated the impact of charge interactions between the weakly crosslinked third network, the negatively charged primary network, and the lubricating medium on lubrication. The strong, attractive forces between the cationic third network and the primary network not only substantially improved hydrogel stiffness but also, together with the third network's internal repulsion, promoted the formation of a stable surface hydration film. This not only strengthened boundary lubrication but also enabled a transition to hydrodynamic lubrication, with a CoF of 0.02–0.05.

4.1.3. Management of reactive oxygen species

Reducing the scaffold porosity can effectively reduce oxygen permeability, but it does not mitigate endogenous ROS produced by damaged tissues and may simultaneously hinder nutrient supply within the scaffold.[107] The scavenging of ROS primarily relies on scaffold materials and the loading of tissue regulators, which operate through two main pathways: promoting ROS metabolism and reducing ROS production (Figure 3D).[7,131,132] Effective ROS-resistant strategies have been widely studied in OA treatment, with common ROS-scavenging agents including vitamin C, phenols (e.g., vitamin E, glycyrrhizic acid), ubiquinones (e.g., coenzyme Q), glutathione, carotenoids, xanthan gum, kartogenin, resveratrol, curcumin, epigallocatechin gallate, lignin, and tannic acid.[73,133-135] Additionally, novel nanozymes such as CeO_2, MnO_2, and Mn_3O_4 can act as catalysts to promote ROS metabolism, exhibiting greater stability and lower cost compared to natural enzymes.[131] Some GFs, such as BMP-2, TGF-β1, and VEGF, also have antioxidant effects.[136] Whether delivered by direct injection or scaffold loading, these agents show good ROS-scavenging effects to promote tissue regeneration and slow degradation, and integrating ROS-sensitive linkages (e.g., thioether, ketal, boronate ester bonds) allows for ROS-responsive release.[135,137,138] Furthermore, self-antioxidant scaffolds can be directly constructed through rational material design: for instance, zinc ions, manganese ions, and magnesium ions can participate in ROS degradation

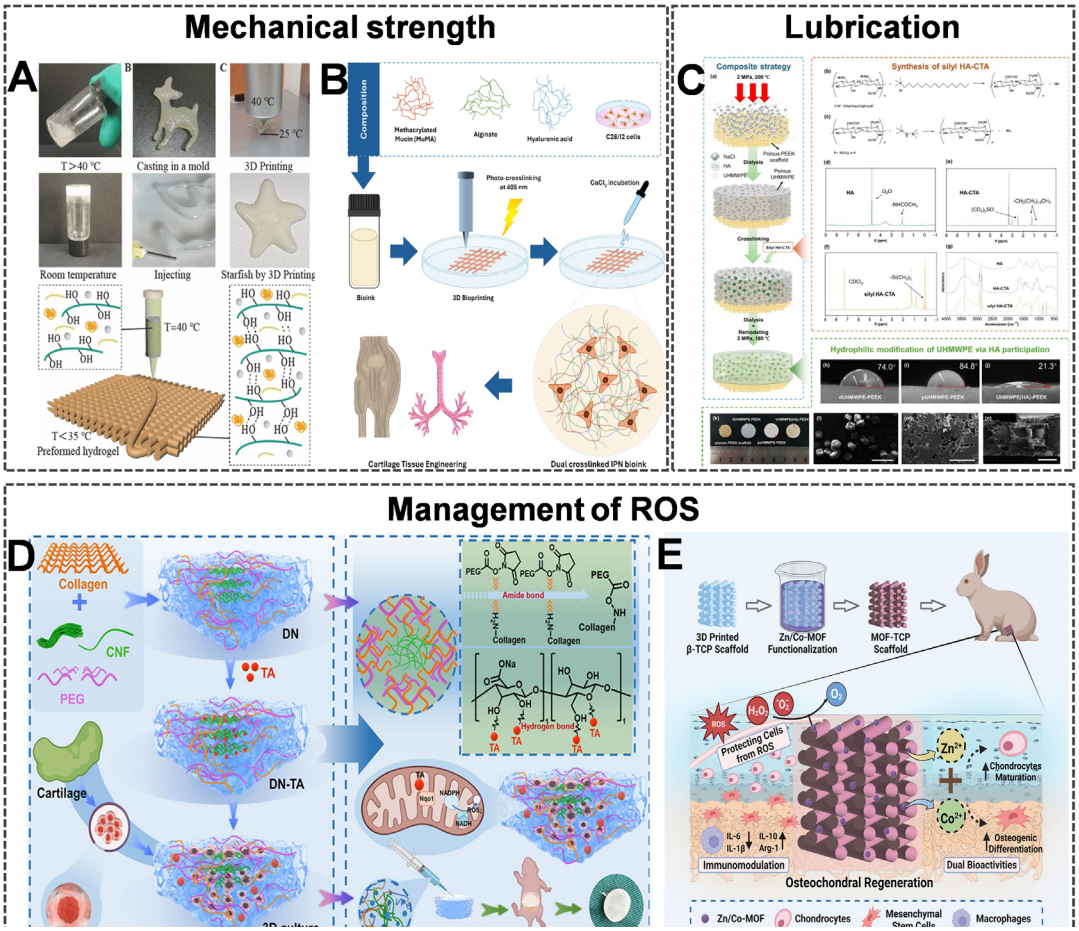

Figure 3. Applications of three-dimensional (3D)-printed scaffolds in hyaline cartilage. (A) The preparation of preformed hydrogel. Reproduced with permission from Yang *et al.*[120] Copyright © 2023, Royal Society of Chemistry. (B) Representative schematic of interpenetrating polymer network (IPN) bioink synthesis and 3D bioprinting. Reproduced with permission from Sasikumar *et al.*[118] Copyright © 2025, American Chemical Society. (C) The fabrication process of the scaffold with continuous hyaluronic acid (HA) supply. Reproduced with permission from Li *et al.*[128] Copyright © 2025, American Chemical Society. (D) Antioxidant functionalized double-net (DA)/tannic acid (TA) dynamic hydrogel for cartilage regeneration. Reprinted from Wu *et al.*[7] (E) Illustration diagrams of metal–organic framework tricalcium phosphate scaffolds in treating osteochondral defects caused by osteoarthritis (OA). Reprinted from Shu *et al.*[139]

reactions, while natural polymers like alginate, chondroitin sulfate, and HA have been validated to alleviate oxidative stress (Figure 3E).[138,139]

Because oxidative stress-induced MSC senescence and differentiation inhibition, the application of these antioxidative strategies is critical for enhancing regeneration outcomes. For example, Chen *et al.*[133] optimized xanthan gum's stability and mechanical strength via methacrylation, using it to make cartilage scaffolds by EBP. These scaffolds not only scavenge ROS directly but also promote intracellular endogenous antioxidant enzyme synthesis, avoiding fibrosis and regenerating HAC successfully. Zhu *et al.*[140] used modified natural fucoidan to build scaffolds via DLP, which cleared 94.7% of intracellular ROS efficiently and promoted COLII synthesis. Beyond cartilage TE, ROS regulation also plays a pivotal role in bone regeneration. Sun *et al.*[134] developed a bioink by combining the antioxidant properties of zinc ions, manganese ions, and glycyrrhizic acid, fabricating bone scaffolds via EBP and tripling the regeneration rate. Wang *et al.*[135] constructed ROS-activated OC scaffolds using LDM; kartogenin in the cartilage layer and BMP-2 in the bone layer can be released by ultrasonic stimulation to promote chondrogenesis and osteogenesis, enabling the dual regeneration of HAC and SBP within eight weeks.

4.2. Fibrocartilage

The TMJ condyle is covered by a specialized fibrocartilage, which is crucial for its function and presents a considerable challenge for regeneration. Despite this, most existing

TE approaches for TMJ cartilage regeneration do not distinguish this fibrocartilaginous layer and instead utilize strategies developed for HAC. Given the shared fibrocartilaginous nature, insights into regenerating the TMJ condylar surface fibrocartilage may be gleaned from the more extensively studied and advanced fields of TMJ disc and meniscal TE. Thus, this section will also explore existing 3D printing-based techniques and strategies for regenerating fibrocartilaginous tissues, offering valuable insights for the TMJ condyle.

4.2.1. Temporomandibular joint condylar cartilage

For the fibrocartilage of the TMJ condyle, current TE methods are still in the early stages.[141] However, there are several valuable studies regarding the key factors involved in its regeneration.[53,54] For cell sources, various MSCs exhibit fibrogenic differentiation capacity. Notably, a distinct population of MSCs, abundantly identified within the condylar SZ named fibrogenic MSCs, has further validated the feasibility of acellular scaffold-based tissue regeneration through homing effects.[57] To induce fibrogenic differentiation, various GFs are commonly employed, with insulin-like growth factor-1 and TGF-β1 being the most prevalent, effectively enhancing cell proliferation and ECM synthesis.[142] In addition, connective tissue growth factor functions as a pro-fibrogenic factor and has exhibited excellent efficacy in inducing the cellular secretion of COLI.[55] Scaffolds remain the core of TE. For inducing the regeneration of superficial fibrocartilage, existing scaffold designs primarily focus on regulating cell morphology (rounded/flattened/spindle-shaped). For instance, Yu *et al.*[143] fabricated a biphasic scaffold by adjusting its pore size, porosity, and hydrophilicity, achieving the regeneration of HAC and fibrocartilage. Helgeland *et al.*[141] utilized EBP to fabricate gelatin scaffolds with a pore size of 346 μm and a porosity of 93%. These scaffolds were then permanently crosslinked with genipin to enhance their mechanical properties. When MSCs were seeded on the scaffolds, they exhibited a flattened morphology and produced COLI. Dufour *et al.*[144] used FDM to produce micro-scale PCL fibers, forming a gradient transition in condylar cartilage. Unlike the dense bottom fiber network, which induces spherical cells, the superficial network has smaller fibers and larger spacing, creating a less constrained environment. This promotes cell flattening and abundant COLI secretion.

4.2.2. Temporomandibular joint disc

Research on TMJ fibrocartilage has primarily focused on the TMJ disc. The COL fibers form a circumferential ring around the disc's periphery, with anteroposterior alignment consistently observed throughout the intermediate band.[55,145] Notably, some researchers contend that the TMJ disc shares a common origin with the condylar fibrocartilage.[52] Adjusting cell morphology is also a common technique utilized in TMJ disc regeneration. Yi *et al.*[146] fabricated a scaffold framework with a pore size of ~350 μm via EBP using PCL and polyurethane. The framework was then modified with polydopamine and TMJ disc-derived dECM to modulate hydrophilicity and provide biochemical signals. After six weeks, regular and dense COLI fiber deposition was observed. Furthermore, a major focus in TMJ disc TE is the biomimetic replication of its fiber arrangement. This approach not only promotes the directed migration of cells but also facilitates the simulation of the mechanical microenvironment.[147] Direct decellularization of the TMJ disc for scaffold fabrication is a convenient approach, with some successful trials documented.[148,149] Nevertheless, recent studies have demonstrated that decellularization treatments can induce damage to the COL fiber network of the TMJ disc, adversely affecting its physiological properties and mechanical functions.[150] The high controllability of 3D printing makes it an ideal choice for manufacturing such bionic scaffolds. The Lee research group[145,151] has pioneered fibrocartilage disc regeneration via this method for more than 10 years. In 2025, based on a laser-scanned model of the TMJ disc, they utilized multi-material 3D printing, using gelatin as the base, PCL fibers to mimic native-like fiber orientation, combined with the regional delivery of GF-loaded microspheres, successfully regenerating fibrocartilage with a fiber distribution similar to the native TMJ disc *in vivo*.[145]

4.2.3. Meniscus

The meniscus plays a pivotal role in the knee joint by absorbing impact forces, transmitting mechanical loads, lubricating cartilage surfaces, and ensuring joint stability.[152] Its peripheral region is primarily structured with circumferentially and radially oriented COLI fiber bundles, which are critical for conferring both tensile and compressive strength.[153] As one of the most prevalent knee joint diseases, meniscal injury creates a strong demand for regenerative technologies, making the meniscus a primary target in fibrocartilage regeneration with deep integration of 3D printing.[154] For meniscal TE, regulating cell phenotype and mimicking the endogenous fibrous network are also well-established scaffold design strategies. Importantly, emulating the internal COLI arrangement of the native meniscus has been proven effective in improving mechanical performance and exerting a direct regulatory effect on cell alignment.[147]

Furthermore, incorporating COLI into scaffolds represents a clinically relevant approach to induce

fibrocartilage formation in meniscal TE. Kremer *et al.*[154] found that supplementing COLI into dECM boosted cellular COLI secretion, and the cells' gene phenotype was highly similar to native meniscal tissue. Savin *et al.*[153] observed that cells on COLI-incorporated scaffolds became spindle-shaped, elongated, and aligned along COL fibers, with improved proliferative activity. As such, COLI serves as a highly biocompatible cell-adhesive material and effectively constructs a regenerative microenvironment tailored for fibrocartilage formation.[154,155] Notably, the clinically approved meniscal regenerative scaffold collagen meniscus implant (Menaflex, formerly known as CMI) comprises 97% COLI.[153] Capitalizing on the manufacturing advantages inherent to 3D printing, Shen *et al.*[152] incorporated COLI into PCL and fabricated meniscal scaffolds with circumferential and radial fibrous architectures via LDM, thereby achieving dual biomimicry of both composition and structure. *In vitro* studies confirmed that fibrocartilage cell proliferation increased with rising COLI concentrations in the scaffolds, while *in vivo* data showed that the regenerated tissue was highly comparable to the native meniscus at three months.

5. Three-dimensional printing-based fabrication of bone scaffold

5.1. Mechanical strength

5.1.1. Composite material

Cancellous and cortical bone scaffolds play a crucial role in energy transfer and dissipation, necessitating exceptional mechanical strength to preserve the scaffold's mechanical inductive functionality and structural stability.[8,67] Thus, metals and bioceramics are favored in bone TE over cartilage TE, underscoring the need for sophisticated composite material design.[77,83,94] The development of materials for bone scaffolds is a thriving area of research. Beyond conventional material compounding techniques, leveraging 3D printing's inherent multi-channel and multi-material fabrication benefits has facilitated the creation of an increasing number of composite bone scaffolds.[34,88] Most notably, synergistic composites composed of rigid and flexible materials are the primary focus—these two components are deliberately designed to respectively satisfy the mechanical and bioactivity requirements of the scaffold, while exhibiting highly controllable directed deposition capacities.[85,91,95,119] Yao *et al.*[156] developed multi-material bone scaffolds with tunable COL/PCL ratios: PCL, compatible with high-precision printing, acts as a rigid framework that is efficiently embedded with COL filaments, while concurrently conferring structural stability to the scaffold (Figure 4A). Gupta *et al.*[157] proposed a multi-material manufacturing strategy named load-bearing 3D bioprinting, wherein calcium phosphate cements constitute the load-bearing component, successfully enhancing the scaffold strength to match that of native cancellous bone. The tailored thermoreversible ion-covalent entangled bioink facilitates the retention of cell viability and reinforces interfacial bonding between the two materials. Liang *et al.*[158] developed a silk fibroin-based composite scaffold via an "organic–inorganic assembly" strategy: ethanol-induced β-sheet enrichment in silk fibroin hydrogel serves as a flexible bioactive matrix, while *in situ* HAP acts as the rigid component, jointly boosting the compressive modulus to 2.33 MPa and enabling efficient regeneration of weight-bearing bone defects *in vivo* (Figure 4B).

5.1.2. Anisotropy

Base material selection and compositional design form the cornerstone for realizing mechanical strength, while pore control serves as the key to further replicating the characteristics of natural bone.[86] From a mechanical standpoint, it not only regulates the overall mechanical strength of the scaffold but also acts as a critical strategy to mimic bone anisotropy, enabling advanced biomimicry.[96,106]

For cancellous bone, conventional scaffold designs primarily emphasize its high porosity, relying on regular geometric configurations. While these designs can macroscopically simulate cancellous bone, their internal stress distribution is suboptimal.[60,109] In 2014, Cheng *et al.*[62] reconstructed cancellous bone via computed tomography scanning and utilized it as a template to fabricate scaffolds through SLS. A significant enhancement in the osteogenic differentiation of cells was observed *in vitro*. However, despite its high biomimicry, the irregular trabecular structure of this forward modeling method demands high printing precision, making local defects prone to occur and limiting parameter flexibility. With technological advancements and a deeper understanding of trabecular bone, researchers in recent years have endeavored to simulate its anisotropic structure via inverse modeling, topology optimization, and mathematical methodologies, with Voronoi Tessellation emerging as the dominant mathematical approach.[60,159] The Voronoi algorithm is particularly adept at simulating natural features due to its inherent nearest-neighbor and adjacency characteristics. Scaffolds manufactured by precisely adjusting the distribution of seeds and scaling factor can achieve a directional arrangement that is highly consistent with natural cancellous bone.[109,160,161] Through Voronoi algorithm-based modeling, Liang *et al.*[160] constructed irregular trabecular-like scaffolds using PBF. Simulation results indicated that although the irregular structure led to a reduction in the scaffold's fatigue durability, its fluid behavior was highly similar to that of natural

cancellous bone, which comprehensively enhances the scaffold's osteogenic induction capacity. Luo *et al.*[161] parameterized images obtained via computed tomography using the Voronoi algorithm, optimized the design through finite element analysis (FEA) and computational fluid dynamics simulation, and successfully fabricated Ti-6Al-4V cancellous bone scaffolds via SLM (Figure 4C). Furthermore, the surface of the scaffolds was modified with an exosome-loaded hydrogel coating. Validation results demonstrated that the porosity, average pore size, and the trabecular network with a trabecular thickness of these scaffolds were close to those of natural cancellous bone. Meanwhile, uniform internal stress distribution with a pressure gradient provides high mechanical stability and efficient fluid transport.

Mimicking the pore structure of cortical bone is also an advanced scaffold design strategy. Simulating the outward–inward pore gradient variation of cortical bone has been widely applied in integrated cortical–cancellous bone scaffolds fabricated via 3D printing, exhibiting excellent mechanical stability.[68,90] Furthermore, mimicking the hierarchical pore structure of cortical bone further reconciles the competing demands for mechanical properties, scaffold surface area, and vascularization channels.[162] Macropores are typically directly fabricated via 3D printing, while micropores often require additional techniques such as particle leaching, phase separation, and gas foaming.[105] Sun *et al.*[67] demonstrated the preparation of hierarchical porous polyetheretherketone bone scaffolds by combining LDM with phase separation technology: LDM was used to fabricate micron-scale macropores, while solvent evaporation induced the formation of nano-scale micropores, which not only adjusted the scaffold strength but also significantly increased its surface area. Recently, Lee *et al.*[162] reported a fully 3D printing-based fabrication strategy for hierarchical porous bone scaffolds. Utilizing a precision extrusion deposition head system and a grid-in-grid structure design, they successfully fabricated hierarchical porous scaffolds featuring global pores (500 μm) and local pores (50–200 μm). This solvent-free 3D printing approach not only enables precise control over pore sizes and ensures high pore interconnectivity but also generates surface topographical cues through the inherent high curvature of local strands and optimized micro-wrinkle structures, thereby guiding cell behavior.

5.2. Prevascularization

Vascular formation and maturation are prerequisites for osteogenesis. Thus, Kuss *et al.*[85] introduced the concept of "prevascularization" in 2018, highlighting the importance of inducing angiogenesis through GFs and optimizing scaffold porosity, particularly pore size and interconnectivity, in bone TE. Regarding GFs, controlled sequential release is widely recognized in bone TE, given the importance of prevascularization. Hypoxia-inducible factor-1α, VEGF, and fibroblast growth factor are primary angiogenic factors; their preferential release has been shown to effectively enhance the efficiency and success rate of subsequent osteogenic processes.[33,113] For scaffolds, computational simulation models have revealed that vascularization efficiency increases significantly with pore size within the 40–270 μm range.[85] Currently, it is widely accepted that an ideal pore size for angiogenesis should exceed 300 μm.[68,95] Additionally, high pore interconnectivity is essential for scaffolds, necessitating sophisticated channel design.[29,104] Traditional manufacturing methods, including microfabrication and soft lithography, have demonstrated inherent limitations in the fabrication of such channels.[102] Conversely, 3D printing, the most advanced vascular regeneration technology, has seen extensive exploration in bone TE.[76,113] Among the various channel designs proposed, biomimetic Haversian systems have emerged as a highly effective approach. The Wu research group[64,102] has conducted extensive investigations into 3D-printed biomimetic Haversian systems, starting from simple biomimetic Haversian canals and advancing to the addition of transverse Volkmann canals (Figure 4D). These advancements have not only optimized angiogenesis but also improved the mechanical properties of the scaffolds and enhanced their osteogenic efficiency. Ghobadi *et al.*[68] demonstrated that vascularized bone scaffolds created through forward modeling and parameter design showed that scaffolds with intricate anatomical features, such as a vertical–horizontal–radial–central microchannel layout, displayed superior angiogenesis, mechanical properties, and cell viability.

Moreover, drawing inspiration from the angiogenic capacity of the periosteum's outer fibrous layer, researchers have recently investigated artificial periosteum as a functional element in bone regeneration.[12] For example, Tariq *et al.*[163] developed a periosteal scaffold with an outer vascular layer doped with magnesium and zinc oxide nanoparticles to boost angiogenesis. Zhao *et al.*[71] created a periosteum bone-mimicking bilayer scaffold, incorporating a DN hydrogel outer layer inspired by bone's endogenous electrical properties. This layer enhanced vascularization via synergistic piezoelectric stimulation across multiple pathways. Feng *et al.*[164] reported a 3D-printed bilayer periosteal scaffold, where the microporous architecture of the outer layer functioned as channels for angiogenesis and, in conjunction with incorporated magnesium ions, effectively promoted initial vascularization.

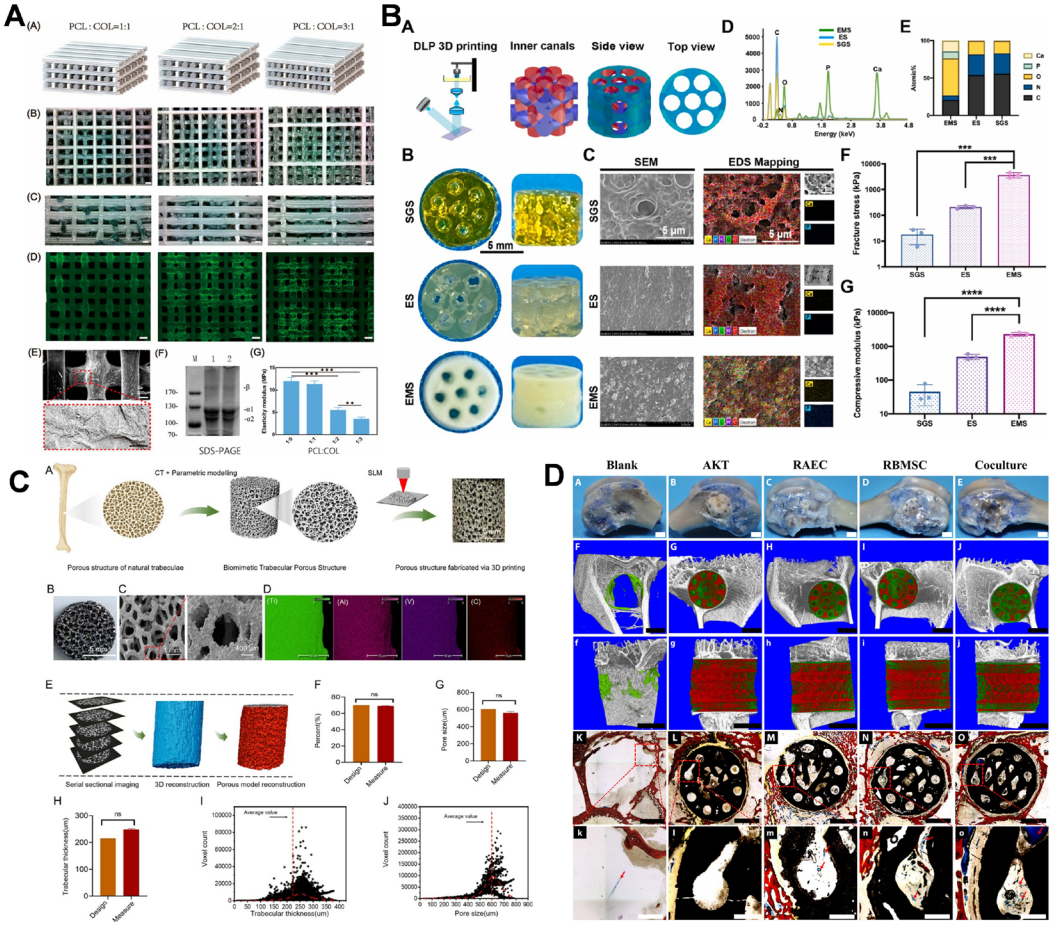

Figure 4. Applications of three-dimensional (3D)-printed scaffolds in bone. (A) Design, printing, seeding, and mechanical strength testing of the hybrid scaffold. Scale bar: (B–D): 500 μm. Reprinted from Yao *et al.*[156] (B) The "organic–inorganic assembly" strategy enhances the mechanical properties of haversian bone-mimicking silgel scaffolds fabricated using digital light processing (DLP). Reproduced with permission from Liang *et al.*[158] Copyright © 2024, Authors. (C) Characterization of biomimetic trabecular design and selective laser melting (SLM) 3D printing scaffolds. Scale bar: 5 mm in (B), 400 μm and 1 mm in (C), 50 μm in (D). Reprinted from Luo *et al.*[161] (D) The Haversian bone-mimicking bioceramic scaffold-based rabbit bone marrow mesenchymal stem cells–rabbit aortic endothelial cells coculture system enhanced the formation of new bone and new blood vessels. Scale bar: 3 mm in (A-E, F-J, f-j), 2 mm in (K-O), 500 μm in (k-o). Reprinted from Zhang *et al.*[64]

6. Three-dimensional printing-based fabrication of osteochondral interface-integrated scaffold

6.1. Discrete gradient scaffolds

Although unidirectional cell differentiation can be achieved by regulating the addition of cells and GFs in monophasic scaffolds, homogeneous scaffolds are unable to meet the distinct biochemical and mechanical requirements of bone and cartilage.[2] The structural and functional differences between these tissues require OC scaffolds to have a regionalized design to suit their specific regenerative requirements.[22] Discrete gradient scaffolds have thus been developed, involving the separate construction of individual components followed by integration.[29] First applied in 2004, OC discrete gradient scaffolds benefit from regional fabrication, allowing a wider material selection and diverse manufacturing approaches while restricting interregional cell migration, thus enabling high regional specificity.[165] Integrating 3D printing simplifies the fabrication of discrete gradient scaffolds and enables more complex designs.[73]

Currently, the most common discrete gradient scaffolds are biphasic scaffolds designed to distinguish between bone and cartilage phases.[139] Liu *et al.*[166] systematically classified the design strategies of OC biphasic scaffolds into three distinct categories: biphasic scaffolds with same material composition ratios but different structural

configurations (SM/DS-biphasic scaffolds); biphasic scaffolds with different material composition ratios but the same structural design (DM/SS-biphasic scaffolds); and biphasic scaffolds with both different material composition ratios and structural designs (DM/DS-biphasic scaffolds). Among these categories, DM/SS-biphasic scaffolds and DM/DS-biphasic scaffolds are the most frequently utilized combinations, primarily attributed to their superior regional induction effects. DM/SS-biphasic scaffolds primarily focus on the role of materials in TE; following long-term development, they have evolved from simple two-phase splicing to manufacturing approaches that incorporate different specific inductive materials into a single base material.[139] Utilizing a single base material for both phases significantly enhances interface bonding strength, and the integrated molding technology provides a continuous framework for biphasic scaffolds, thereby further improving scaffold stability (Figure 5A).[11,114] Building upon the foundation of DM/SS-biphasic scaffolds, DM/DS-biphasic scaffolds incorporate tissue-specific structural designs.[166] With the aid of 3D printing, this fabrication process has been significantly streamlined. Bai *et al.*[167] developed a DM/DS-biphasic scaffold via multi-material sequential cryogenic 3D printing: gelatin-based supramolecular hydrogel served as the common phase, the bone phase contains TCP with a grid structure, while the cartilage phase has a complementary grid structure. *In vivo* experiments showed that the scaffold achieved seamless integration with host tissue and regenerated high-quality OC tissue within three months (Figure 5B). Golebiowska *et al.*[2] fabricated biphasic scaffolds with different filling densities through an integrated 3D-printed PLA framework, where mechanical properties were adjusted by mimicking the pore sizes of natural bone and cartilage.

However, discrete gradient scaffolds represent a highly generalized design of OC tissue. Owing to the mechanical strength disparities between individual phases, issues such as poor interface bonding and stress concentration are prone to occur, thereby compromising scaffold stability.[166,168] To address these challenges, researchers have primarily focused on enhancing the biomimicry of natural tissues. For instance, an intermediate layer mimicking the CCZ has been incorporated into biphasic scaffolds to facilitate smooth stress transition and inhibit vascular invasion from the bone phase into the cartilage phase (Figure 5C).[73,169] Although augmenting the layers can enhance the performance of distinct gradient scaffolds, the interface remains, thereby precluding the complete elimination of interface bonding issues.[2] For example, in a study by Kotlarz *et al.*[169], the scaffold was constructed with a bone phase of Ti-6Al-4V fabricated via PBF and a cartilage phase consisting of a bilayer hydrogel system. However, while this scaffold exhibited promising regenerative outcomes *in vitro*, it still encountered issues such as insufficient osseointegration, cartilage tissue degradation, and poor mechanical stability *in vivo*.

6.2. Continuous gradient scaffolds

The constraints of discrete gradient scaffolds have motivated researchers to pursue alternative approaches. Similar to the design of shock-absorption systems in engineering, achieving robust integration and mechanical reconstruction of OC tissue requires scaffolds with graded compositional or structural transitions by adjusting material ratios or microstructures, thereby avoiding interfacial stress concentration[72,91,170](Figure 5D). Golebiowska *et al.*[2] conducted experiments that revealed gradient scaffolds had better mechanical absorption properties than various multiphasic scaffolds. The internal stress changes in these gradient scaffolds were continuous and smooth, closely matching those found in natural OC tissue. Although several fabrication methods can be employed to create gradient scaffolds, 3D printing stands out due to its ability to provide rapid, high-resolution control over the scaffold's internal geometry. As such, it is currently regarded as the most suitable fabrication method for the production of continuous gradient OC scaffolds.[166,171]

For OC scaffolds with material gradients, COLs and HAP are the most prevalent materials employed, as they respectively promote chondrogenesis and osteogenesis. Beyond providing crucial biochemical signals to cells, these materials also help tailor the scaffold's mechanical properties, aiding in the creation of mechanical strength gradients.[70] Xiao's group[70,171] used 3D printing to develop BioGradCart, an OC scaffold with gradient COL and HA distributions. Through continuous improvement, this scaffold has shown superior biomimetic and regenerative performance. In another study, Yang *et al.*[4] created hydrogel inks for HAC, CCZ, and SBP using methacrylic acid as the base. Using DLP, they fabricated an integrated OC scaffold with gradients of ColI, ColII, and HAP. This scaffold overcame delamination and mechanical mismatch, achieving precise reconstruction of natural OC tissue.

Pore size is the most prevalent feature for OC scaffolds with a gradient structure.[166] By adjusting pore sizes, these scaffolds can satisfy the demands of different TE processes, such as cell migration, oxygen concentration, and channel availability.[22] Nowicki *et al.*[168] used FDM to create a continuous filling density gradient in scaffolds, achieving anisotropic pore distribution and effectively eliminating stress concentration. Sun *et al.*[5] utilized 3D printing to control PCL fiber spacing, which gradually varied from 150 μm to 750 μm, delivering differentiation signals for

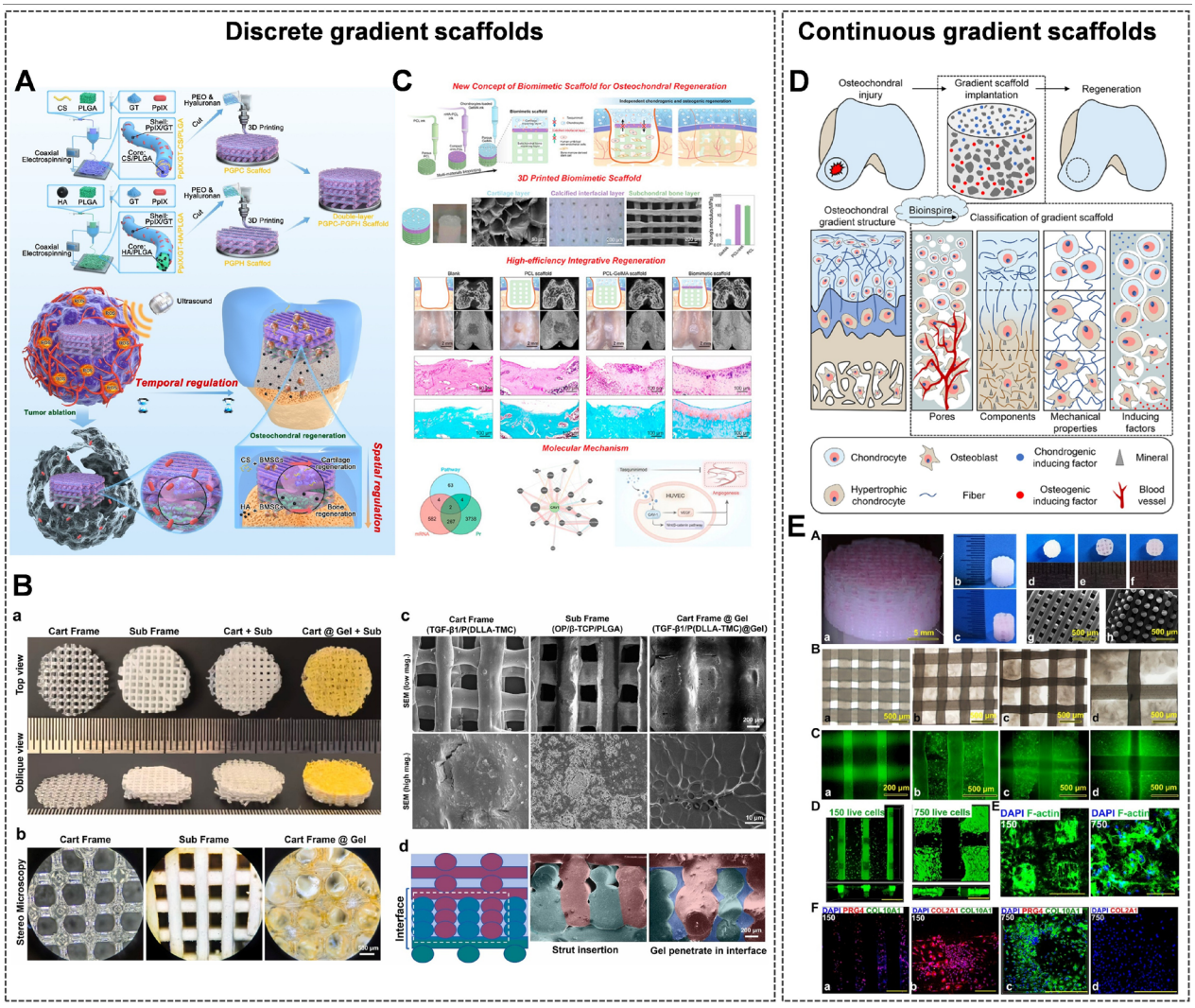

Figure 5. Applications of three-dimensional (3D)-printed scaffolds for osteochondral (OC) regeneration. (A) A 3D-printed biomimetic scaffold with a calcified interfacial layer, which acts as a compact barrier between the cartilage layer and subchondral bone layer. Scale bar: 50 μm, 200 μm, 200 μm (corresponding to the microstructural images). Reproduced with permission from Wu *et al.*[73] Copyright ©, 2024 Authors. (B) Creation of a double-layer PGPC–PGPH porous scaffold, with the upper layer consisting of protoporphyrin IX (PpIX)/gelatin (GT)–chondroitin sulfate/poly(lactic-co-glycolic acid) (PLGA) ink and the lower layer comprising PpIX/GT–hyaluronic acid/PLGA ink. Reproduced with permission from He *et al.*[114] Copyright © 2023, Authors. (C) Morphology of cryogenic 3D-printed OC scaffolds with heterogeneous structure. Scale bar: 500 μm (b); 100 μm, 10 μm (c); 200 μm (d) Reproduced from Bai *et al.*[167] (D) A 3D-bioprinted gradient cartilage scaffold with microchannels between polycaprolactone (PCL) fibers, with widths that ranged from 150 μm to 750 μm. Scale bar: 5 mm (A-a); 500 μm (A-g/h, B-a-d, C-b-d); 200 μm (C-a). Reproduced from Sun *et al.*[5] (E) Schematic illustration of bioinspired scaffolds with gradient pores, components, mechanical properties, and inducing factors for osteochondral repair. Reproduced from Peng *et al.*[170]

cartilage and bone (Figure 5E). This approach successfully regenerated tissue and restored cartilage anisotropy and bone vascularization. Beyond pore size, modifying scaffold internal geometry can also mimic the mechanical transition of OC tissue. Eckstein *et al.*[91] varied the geometry within a repeating octet truss unit-cell structure to spatially vary stiffness and replicate compressive strain gradients that are characteristic of OC tissue. The scaffold, fabricated via modified SLA and filled with hydrogel, closely matched the mechanical properties of natural OC tissue.

7. Application of artificial intelligence in the three-dimensional printing of osteochondral scaffold

In OC TE, AI mainly provides assistance in three aspects, including the precise regulation of printing process parameters, the optimized development of ink formulations, and the rational optimization of scaffold structure (Figure 6).

7.1. Artificial intelligence-assisted optimization of three-dimensional printing parameters

Three-dimensional printing relies on numerous preset parameters, from basic ones like printing speed, layer thickness, scanning path, and support structure to special settings, such as nozzle size, nozzle temperature, and laser power.[61,81,172] These are key factors affecting geometric accuracy, interlayer bonding strength, and material compatibility.[90,173] As material development demands grow, printing systems critically need adaptive adjustments based on material properties.[156] This need has driven the use of AI, especially ML, which efficiently matches ink performance and optimizes multiple parameters in 3D printing.[174] ML-based printing parameter optimization generally involves three steps: first, sensors extract and quantify features of the printing process and products; second, raw data is used to build a model mapping parameters to product quality; and finally, simulation and prediction help find the best parameter combination.[175] After ML makes optimal decisions, classical AI combines with presets to generate and execute adjustment instructions, forming a closed-loop system for *in situ* adaptive control of printing.[21] Due to ML's reliance on high-quality datasets, feature acquisition, analysis, and processing—the first step and foundation of raw dataset formation—is now a major driver of parameter optimization in 3D printing.[173,176] Computer vision systems (CVS), as a low-cost, non-contact visual imaging tool, play a central role in this process.[177] Based on image data acquired via CVS, ML models apply algorithms like naive Bayes, k-nearest neighbors, and

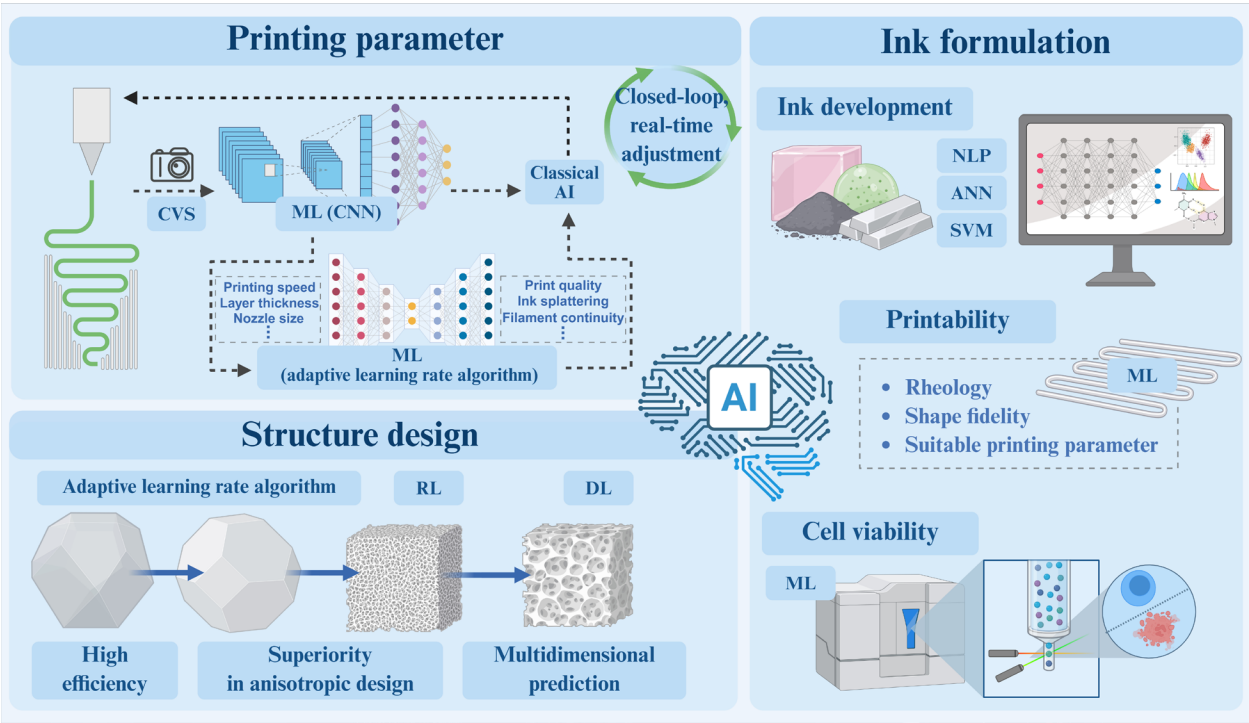

Figure 6. Artificial intelligence (AI)-assisted three-dimensional printing in osteochondral tissue engineering
Abbreviations: ANN: Artificial neural network; CNN: Convolutional neural network; CVS: Computer vision system; DL: Deep learning; ML: Machine learning; NLP: Natural language processing; RL: Reinforcement learning; SVM: Support vector machine.

decision trees to compare and quantify products against predefined patterns based on resolution, integrity, and other features.[14,172] Among these, deep learning (DL)-based convolutional neural networks (CNNs) are the most effective ML models for image processing, finding broad use in optimizing 3D printing parameters.[98,173] As a core ML technique, DL uses the multi-layer artificial neural network (ANN) to process raw data directly, with built-in algorithms enabling nonlinear information iteration across layers. It offers exceptional data processing and generalization, excelling at unstructured data like images, audio, and text.[174] CNN, a specialized ANN for grid-structured data, is widely used in image processing and aligns well with the technical demands of CVS.[14,177] By mimicking the biological visual system's mechanism of "local feature extraction to holistic perception," CNN can utilize convolutional filters to identify and track region-of-interest features in images captured by CVS, thereby generating corresponding feature maps. Subsequent pooling operations downsample the data while preserving invariance to small shifts and distortions. These feature maps undergo iterative refinement through successive convolutional and pooling layers, and are ultimately flattened into one-dimensional vectors via the fully connected layer for global feature integration, providing data-driven support for the optimization of subsequent printing parameters.[173,175,176,178]

For instance, Chung *et al.*[21] combined CNN with classical AI to form a feedback system: after detecting and classifying defects in PBF-printed ceramics, they correlated defective surfaces with overall print quality and performed re-evaluation, effectively addressing shrinkage and microcracks in ceramics. Beyond classical AI, CNN can be further integrated with ML, with the adaptive learning rate algorithm being a key integration point.[175,176] This algorithm dynamically assigns personalized learning rates to each parameter based on the gradient statistical characteristics of parameters during model training.[179] Endowed with fast convergence, strong robustness, and multi-objective optimization capabilities, it is currently the core ML optimization algorithm and one of the most common prediction algorithms in 3D printing parameter optimization.[180] Based on CNN-derived image segmentation and classification results, Jin *et al.*[175] compared various ML algorithms, selected the adaptive learning rate algorithm for its optimal efficiency, and established an anomaly detection system for 3D-printed scaffolds with an overall accuracy over 90% across different infill patterns. Going beyond print result evaluation, Shi *et al.*[176] utilized CNN to model the nonlinear relationship between single droplet evolution in PIJ-based bioprinting and printing parameters. Using the adaptive learning rate algorithm, they optimized the voltage for multiple bioinks (single-objective) and balanced ink viscosity with printing parameters (multi-objective).

7.2. Artificial intelligence-assisted three-dimensional printing ink formulation

While there is abundant research on OC scaffold materials, traditional design methods remain hampered by their reliance on sequential empirical parameter optimization, which lacks intelligent forecasting and integrated planning.[77,94] This inefficiency means new materials can take years to move from lab to clinic. At the information acquisition stage, ML can utilize chemical databases or mine multimodal data from the literature through natural language processing (e.g., Transformer-based text extractors and topic modeling algorithms), to directly extract multimodal data from literature and convert it into standardized features, thereby drastically shortening the cycle of material development, optimization, and testing.[15,181] Moreover, ML models like ANN and support vector machine (SVM) excel at capturing complex nonlinear correlations from standardized features to build precise feature-performance mapping models, with respective strengths in large-scale and small-sample data processing.[15] For instance, Li *et al.*[182] developed a peptide-based self-assembling hydrogel library using combinatorial chemistry. They then employed ANN and SVM to identify key chemical features and quantify the relationship between molecular structures and hydrogel behavior, thereby creating a powerful tool for predicting and designing peptide hydrogels with optimal peptide motifs. Similarly, Javaid *et al.*[183] integrated multi-criteria decision analysis methods with various ML algorithms, including SVM, to identify and rank the most suitable biomaterials for cortical and cancellous bone TE scaffolds based on three critical mechanical properties: comprehensive strength, tensile strength, and Young's modulus. Their work also involved comparing the predictive efficiency of various ML algorithms, offering valuable insights for the quantification of material properties and multi-objective evaluation. In another study, Ren *et al.*[15] proposed HydrogelFinder, a fundamental model for the rational design of self-assembling peptides, which incorporates a deep neural network composed of a multi-layer ANN. This model integrates the entire workflow from training set construction and modeling the structure–self-assembly relationship to virtual evaluation and screening. Utilizing this approach, they successfully identified nine previously unreported novel self-assembling peptide hydrogels.

For 3D printing, combined with CVS, ML can assess and predict ink printability, optimize print quality by adjusting ink properties, and potentially enable bidirectional

optimization alongside printing parameters.[18] Lee *et al.*[82] used ML to study how a composite's rheology relates to its printability. They pinpointed ink elastic modulus as key for shape fidelity and yield stress as important for nozzle extrusion. Leveraging these insights, they employed multiple regression analysis to develop predictive models for formulating natural bioinks with high shape fidelity. Nadernezhad *et al.*[184] focused on HA-based matrices, using an interpretable ML approach to study the relationship between bulk rheological indices and printability scores. Their work led to the identification of 13 key rheological indices that significantly influence printability, offering a way to overcome the opacity of traditional "black box" ML models. Chen *et al.*[185] accelerated ink development by 3D printing and testing 210 formulations. They trained ML models on this data to predict printability with over 80% accuracy.

Scaffolds are required to exhibit superior biocompatibility in TE. Moreover, the complex printing process imposes elevated requirements on bioink formulations, as they must effectively maintain the viability of encapsulated cells.[18,99] During printing, cell viability is influenced by multiple factors, including material properties and printing parameters.[101] For example, in widely used IJP-based bioprinting and EBP-based bioprinting, the ink's shear-thinning behavior and printing-induced shear stress together challenge cell survival.[74,172] Additionally, highly biocompatible materials often suffer from poor shape fidelity after cell incorporation.[174] Therefore, the optimization of cell-laden bioink formulations demands a careful trade-off between printability and biocompatibility.[183,185] Based on extensive datasets, ML is capable of predicting cell behaviors; by integrating such predictions with the optimization of printing parameters and bioink recipes, it facilitates effective cell protection in 3D bioprinting processes.[187] Xu *et al.*[188] developed a multi-algorithm model to predict cell viability in SLA-based bioprinting by combining ultraviolet intensity, irradiation time, GelMA concentration, and layer thickness. The model revealed complex parameter relationships, supporting high-precision prediction of additional variables. For comprehensive bioink optimization, Zhang *et al.*[189] created a universal method integrating rheological modeling, high-fidelity simulation, and ML. It characterizes cell viability retention across cell types, shear stresses, and exposure times, accelerating bioink formulation accuracy and informing printing parameter optimization. Mohammadrezaei *et al.* [17] trained regression and classification neural networks to predict printing conditions' impact on cell viability. They further combined Bayesian optimization with the regression network to inversely predict viability-maximizing parameters, covering all critical aspects of bioink development.

7.3. Artificial intelligence-assisted structure design of three-dimensional-printed osteochondral scaffolds

Beyond optimizing 3D printing to enhance the precision manufacturing of OC scaffolds indirectly, researchers are actively exploring its exceptional predictive capabilities in the structural design of OC scaffolds to improve both their mechanical performance and biochemical functionality. Simulating cartilage mechanics primarily involves material design: by inputting various mechanical property parameters of natural cartilage, ML can effectively predict the performance of composite materials. For example, Mairpady *et al.*[190] used a multinomial logistic regression algorithm to identify a polyethylene/polyethylene-graft-poly(maleic anhydride) blend as the most promising candidate material for cartilage repair. Although AI research targeting cartilage scaffolds remains limited, it can analyze the complex composition–process–structure–property model to predict various properties of hydrogels, such as mechanical strength, water absorption capacity, and stability, thus demonstrating promising application prospects in the characterization and optimization of hydrogel performance.[191,192,193]

In contrast, the design of bone scaffolds faces the critical challenge of harmonizing structural geometry with desired mechanical functions. This is especially demanding due to the anisotropic characteristics inherent in bone tissue, which impose significant constraints on scaffold design strategies. While various mathematical algorithms, notably the Voronoi algorithm, have been validated for this purpose, their practical application is often hindered by high complexity, rendering them less than optimal.[19,60,160] In this regard, AI emerges as a highly efficient alternative, offering new avenues to tackle these design complexities. Emphasizing the structure-mechanics mapping, a variety of algorithms can be employed in scaffold design, such as the adaptive learning rate algorithm, reinforcement learning, DL methods including CNN, graph neural network, and generative adversarial network.[179,194,195] Kumar *et al.*[63] designed a porous cellular mechanical metamaterial scaffold based on spinodoid topology using a bidirectional mapping model based on a deep neural network. By cross-validating target mechanical performance parameters with scaffold structural parameters to optimize weights, this model addresses the issue of "design and performance disconnect" inherent in traditional unidirectional models, generating scaffolds with highly biomimetic anisotropic elastic stiffness. Liu *et al.*[20] used a shallow ANN called the back-propagation neural network to map structural parameters to mechanical properties. They then embedded

a regenerative genetic algorithm into ML for inverse design, efficiently producing anisotropic TPMS structures. The FEA confirmed this method's accuracy. Shetty *et al.*[196] adopted orthogonal array-driven FEA to efficiently generate a paired database that correlates scaffold structural parameters with mechanical performance. They then trained a back-propagation neural network via an adaptive learning rate algorithm, achieving the optimal geometric type-wall thickness combination. This method reduced invalid experimental trials by over 60% and delivered a practical, reusable algorithm framework for small-sample engineering problems. Wang *et al.*[197] constructed a dual-CNN framework: one replaces the phase-field model to generate spinodal structures, ensuring pore interconnectivity via circular padding technology; the other predicts mechanical properties to support high-throughput screening. Using data augmentation (e.g., rotation, scaling), the model captures pore size-cell migration correlations to generate scaffolds with targeted pore distribution and smooth interfaces, translating abstract structure–property links into practical pore optimizations that improve both mechanical strength and biocompatibility. Furthermore, prevascularization of bone scaffolds stands as a critical challenge in TE. AI has also provided innovative solutions for breakthroughs in this field. Ashkan *et al.*[198] introduced a Q-Learning method based on reinforcement learning—a core ML algorithm that enables an agent to act within an environment, calculate feedback rewards for each action, and solve tasks through trial and error to maximize the cumulative reward. In their work, after reconstructing a 3D bone tissue model from imaging data and screening core slices, Q-Learning was employed to design vascular paths with minimal tortuosity, which, through Bezier curve fitting and 3D rendering, efficiently generates patient-specific vascular networks tailored to the anatomical structure. Although current research on AI applications in bone scaffold prevascularization is still in the exploratory stage, existing studies have demonstrated significant transferability. For instance, Cadle *et al.*[199] utilized the CVS to perform feature extraction and path optimization based on vascular computer-aided design images of rodent mesentery and colon, successfully fabricating TE constructs by 3D bioprinting with both anatomical accuracy and physiological functionality.

Going beyond direct structural design, ML can forecast cell behavior and regeneration by using various scaffold structural features as inputs, enabling inverse scaffold design.[200] Fielder *et al.*[16] used unsupervised ML clustering models, which eliminate the need for labeled data and excel at dimensionality reduction and mining inherent data patterns, to predict OC regeneration efficiency, considering variables like scaffold material and pore shape. These models reveal how different variables impact regeneration, laying a solid theoretical and data-driven foundation for the on-demand scaffold design. Drakoulas *et al.*[201] factored in the *in vivo* environment, using material, stress, and fluid velocity as inputs. They applied a probabilistic ML-based reduced-order model that leverages real physical simulation data for dimensionality reduction and efficient prediction to predict cell type distribution and optimized parameters via non-dominated sorting genetic algorithm II, demonstrating the potential of using reduced-order models for scaffold design optimization. Naga *et al.*[202] utilized a probabilistic Bayesian neural network that calculates the posterior probability distribution of weights through Bayesian inference and possesses robust uncertainty quantification capabilities to predict TE regeneration based on scaffold stiffness and porosity. This predictive system was further extended to forecast scaffold thermal dynamics and the establishment of connective tissue blood capillary networks and COL crosslinking events. Notably, it has high interpretability and accuracy (>80%) in predicting cell behavior in various bone and cartilage scaffolds, thus providing a robust and reliable reference for scaffold design. Table 4 summarizes the AI-assisted strategies targeting the requirements of OC scaffold design.

8. Discussion

The significance of 3D printing in biomedicine is increasingly recognized, as it has emerged as a pivotal technological advancement in TE. Ranging from the

Table 4. Artificial intelligence-assisted strategies targeting the requirements of osteochondral scaffold design

Region	Requirement	Artificial intelligence-assisted solution
Cartilage	Mechanical properties (mechanical strength)	Composite material formulation design; establishment, analysis, and prediction of composition–process–structure–property model; reverse design based on prediction of regeneration efficiency and cellular behavior
Bone	Mechanical properties (mechanical strength with anisotropy)	Establishment, analysis, and prediction of structure–mechanical property mapping model; performance-guided structural design for anisotropy; reverse design based on the prediction of regeneration efficiency and cellular behavior
	Prevascularization	Anatomical imaging data extraction; pathway optimization via algorithms

macro-scale customization of scaffold geometries to the precise manipulation of microarchitectural details, such as scaffold porosity and cell distribution, 3D printing effectively integrates diverse components of TE. This integration enables the more accurate recapitulation of native tissue features and provides enhanced guidance for regeneration processes.[34,82] In the specific context of OC TE, 3D printing has proposed innovative approaches to tackle several major hurdles. Notably, it exhibits distinct advantages in terms of precise control over scaffold pore parameters, the ability to fabricate anisotropic structures that mimic the natural mechanical properties of OC tissue, and the enhancement of integration at the bone–cartilage interface. Simultaneously, the development of a wide array of 3D printing technologies has revolutionized the application of materials, enabling the creation of a tailored mechanical and biochemical microenvironment that supports cellular activities.[75,106] Following the precise deposition capability of 3D printing, smart constructs capable of detecting environmental conditions and stimuli (such as mechanical, chemical, or magnetic stimuli) and responding to them are also rapidly advancing, further expanding the scaffold functions toward drug delivery and pathophysiological monitoring.[203] Currently, 3D-printed dental and orthopedic implants (including splints, prosthetics, and implants) are clinically available, with over 50 products in clinical trials. Among these clinical and preclinical products, Ti and Ti-6Al-4V alloys processed via SLM and SLS dominate the market, followed by polyetheretherketone products manufactured by FDM. These successful clinical translations provide a basis for 3D printing's further expansion into regenerative medicine.[204,205]

While many current attempts show promise, 3D printing in OC TE still faces significant hurdles. Firstly, various fundamental 3D printing technologies inherently possess limitations, such as inadequate resolution, suboptimal interlayer bonding, and compromised cell viability.[62,70,92] Concurrently, they impose stringent requirements on ink properties, including rheological behavior, photosensitivity, and thermal stability.[186,188] Achieving synergistic coordination among technology, ink formulation, and product specifications remains a primary bottleneck hindering the large-scale application of 3D printing. The confluence of these technical shortcomings and material constraints culminates in elevated experimental costs and protracted research and development cycles. Moreover, a variety of advanced modified printing technologies currently suffer from poor accessibility and prohibitively high application costs. Hence, the comprehensive optimization of 3D printing innovation, ink compatibility, and cost management is a critical research focus for its widespread adoption.[19] Additionally, although we now possess precise anatomical and histological information regarding OC tissue, current 3D printing technologies generally only mimic single or partial features.[65] Due to existing limitations in scaffold design principles, achievable 3D printing resolution, and the ability to fabricate complex multi-material structures, some critical features like the cartilage's zonal structure and lubrication, and the bone's hierarchical pores are still in the early, exploratory stages of development.[48,102,160] Apart from these inherent technical limitations, the clinical translation of 3D-printed products also encounters notable bottlenecks in large-scale production and the formulation of regulatory standards. In terms of large-scale production, the personalized customization, high cost, low production efficiency, and sterilization challenges of 3D printing hinder its large-scale clinical translation.[203] Furthermore, insufficient repeatability and robustness of 3D printing processes lead to inconsistencies in product performance across different laboratories, which further hinder scalability.[206] From a regulatory perspective, the diversity of 3D printing technologies and materials used for scaffold fabrication makes regulatory classification and approval challenging. Particularly for 3D bioprinted products, ethical concerns add layers of complexity to regulation.[169] Meanwhile, the difficulty in scaling production further hinders the establishment of unified testing standards and batch validation procedures. Therefore, 3D-printed regenerative medicine products have not yet been widely adopted in clinical practice. Although organizations such as the United States Food and Drug Administration and the International Organization for Standardization published regulatory guidelines and safety standards for 3D-printed medical devices and tissue regeneration products, these standards have not been revised for many years.[207] As a result, the approval cycle for clinical translation of products under the existing regulatory framework can extend to 5–10 years, which severely hampers the commercialization process and the establishment of a sustainable virtuous cycle for industry development.[203] At present, technological innovation remains the critical breakthrough point to address the clinical translation dilemma of 3D-printed scaffolds, as it holds the potential to reduce production costs and improve product quality. It is worth noting that hydrogels for the treatment of OA are the intra-articular regenerative medicine products with the largest number of ongoing clinical trials.[208] The continuous advancement of these hydrogel materials will indirectly promote the integration of 3D printing technology and regenerative medicine.

Advancements in computing power, algorithmic innovation, and the accessibility of big data have positioned

AI as a transformative tool for addressing the inherent limitations of 3D printing.[20,182] In parameter control, material development, and their joint optimization, ML's predictive and decision-making power, paired with classical AI's automated execution, has enabled standardized, efficient intelligent manufacturing via closed-loop systems, such as *in situ* 3D printing with real-time monitoring and adjustment of multiple variables.[98,186,189] Furthermore, AI-driven advanced mathematical modeling techniques are playing a crucial role in scaffold design. By integrating clinical imaging data with a variety of algorithms, these models are able to generate precise, data-informed, and collaborative design solutions that were previously unattainable.[16,184] Leveraging 3D printing technology for the physical instantiation of AI models achieves a new level of multi-dimensional intelligence in both the design and fabrication phases of scaffold production.[200] Going further, AI has also been used to predict scaffold degradation, inflammation, antibacterial effects, and other *in vivo* performance, highlighting the extensive potential of full-process AI-driven approaches in biomedicine.[209,210]

However, while 3D printing theoretically enables the fabrication of structures with arbitrary geometries, technical constraints may introduce discrepancies between the actual product quality and the AI-designed models.[20,62] More importantly, AI-designed scaffolds are usually simulated and validated using computational tools such as FEA and smoothed particle hydrodynamics, not through experimental testing in real biological environments.[20,63,109,201] What is more critical is that AI applications face challenges, such as difficulty in sample acquisition and labeling, high time costs for model training, poor result interpretability, and overfitting.[14,172] In particular, data scarcity has emerged as one of the major barriers to AI development. The samples used in the current research are insufficient in quantity and low in complexity, leading to inadequate model validation.[211] Furthermore, these datasets often carry biases against ethnic minority groups, which further exacerbates the overfitting issue.[212] Meanwhile, the lack of regulatory standards regarding intellectual property and privacy has hindered data acquisition and utilization. Currently, AI research is often conducted within individual hospitals or regions, resulting in poor generalizability.[172] The establishment of a global, large-scale database based on well-defined regulatory standards remains a long-standing challenge that impedes the advancement of AI technologies and their clinical translation.

The integration of 3D printing technologies with AI-powered design and manufacturing workflows in OC TE offers the potential to develop highly biomimetic scaffolds. However, breaking down disciplinary barriers cannot be accomplished merely through technical integration; a deeply integrated collaborative model among clinicians, materials scientists, and engineers is required to translate this potential into clinically applicable outcomes.[19,60] The cornerstone for accelerating the large-scale implementation of technologies and improving regulatory standards lies in technological innovation. To drive tangible progress of these two emerging manufacturing and design tools (3D printing and AI) in OC TE, future research should focus on three prioritized action directions:

(i) Conduct a comprehensive analysis of the physiological structure and function of OC tissues, with the trinity of "structural bionics, mechanical bionics, and biological function bionics" as the central goal for scaffold design and manufacturing, facilitating tissue regeneration and functional reconstruction at defect sites.[29,147,169]

(ii) Establish consensus-based bioink rheology testing standards, a unified database of 3D printing process parameters, and a globally interoperable database of AI models. Eliminate cross-institutional data barriers via standardized interfaces and governance norms to facilitate large-scale application and regulatory standard development.[203,210,211]

(iii) Deepen tech integration and innovation to achieve in-depth convergence of 3D printing with digital technologies and leverage high-quality 3D printing for rapid prototyping and *in vivo* validation of advanced technologies like AI, thereby ensuring design implementation and clinical translation.[201]

With the support of standardized laboratory data, further promoting the construction of a global technological database will not only provide clear guidance for interdisciplinary cooperation but also become a crucial breakthrough that propels scalable and personalized OC TE solutions from laboratory-based research toward clinical application.

9. Conclusion

Three-dimensional printing has comprehensively revolutionized OC TE, enabling more precise and intelligent manufacturing while expanding the application of various materials. As a cutting-edge tool, AI has advanced rapidly in biomedicine and manufacturing, providing enhanced data-driven optimization approaches for 3D printing, thereby minimizing the resource and time costs of preclinical research and accelerating the path to clinical translation. The integration of these two technologies has collectively broadened the development prospects of OC TE. Although their current applications still face

numerous challenges and remain difficult to popularize, we believe these issues will be gradually addressed through continuous research, innovation, and interdisciplinary collaboration. In the future, AI will further drive the evolution of 3D printing technology, enabling intelligent biomimetic solutions and full-process control for OC tissue regeneration, paving the way for the construction of customized, dynamic, and clinically applicable TE systems.

Acknowledgments

None.

Funding

This work was supported by the National Natural Science Foundation of China (No.82301112), the Sichuan Science and Technology Program (No. 2024NSFSC1592), and the Sichuan Provincial Medical Association Youth Innovation Project (Q20250030).

Conflict of interest

The authors declare they have no competing interests.

Author contributions

Conceptualization: Haozhe Chen
Funding acquisition: Haozhe Chen
Visualization: Haozhe Chen, Maoying Yang, Xinyue Tang
Writing–original draft: Maoying Yang, Yurui Tian, Yue Liao
Writing–review & editing: Haozhe Chen, Linyi Zhu

Ethics approval and consent to participate

Not applicable.

Consent for publication

Not applicable.

Availability of data

Not applicable.

References

1. Seims KB, Hunt NK, Chow LW. Strategies to Control or Mimic Growth Factor Activity for Bone, Cartilage, and Osteochondral Tissue Engineering. *Bioconjug Chem*. 2021;32(5):861-878.

   doi: 10.1021/acs.bioconjchem.1c00090

2. Golebiowska AA, Nukavarapu SP. Bio-inspired zonal-structured matrices for bone-cartilage interface engineering. *Biofabrication*. 2022;14(2).

   doi: 10.1088/1758-5090/ac5413

3. Boyde A. The Bone Cartilage Interface and Osteoarthritis. *Calcif Tissue Int*. 2021;109(3):303-328.

   doi: 10.1007/s00223-021-00866-9

4. Yang X, Wang L, Chen X, Ling B, Xiao J. Digital light processing 3D bioprinting of collagen-based gradient osteochondral scaffold for cartilage-bone regeneration. *Int J Biol Macromol*. 2025.

   doi: 10.1016/j.ijbiomac.2025.148403

5. Sun Y, You Y, Jiang W, Wang B, Wu Q, Dai K. 3D bioprinting dual-factor releasing and gradient-structured constructs ready to implant for anisotropic cartilage regeneration. *Sci Adv*. 2020;6(37):eaay1422.

   doi: 10.1126/sciadv.aay1422

6. Xu Q, Huo L, Wei X, *et al*. Clinical application of customized total temporomandibular joint prosthesis by 3D printing: a five-year follow-up study. *Clin Oral Investig*. 2025;29(4):210.

   doi: 10.1007/s00784-025-06260-1

7. Wu X, Wang H, Li C, *et al*. Antioxidant functionalized double-net/TA dynamic hydrogel promotes cartilage regeneration through stabilization of chondrocyte phenotype. *Mater Today Bio*. 2025;34:102203.

   doi: 10.1016/j.mtbio.2025.102203

8. Doyle SE, Snow F, Duchi S, *et al*. 3D Printed Multiphasic Scaffolds for Osteochondral Repair: Challenges and Opportunities. *Int J Mol Sci*. 2021;22(22):12420.

   doi: 10.3390/ijms222212420

9. Yang Q, Chen A, Zhang X, Wu Z, Zhang C. Functional poly(ether-ketone-ketone) composite scaffold with enhanced cell-material interaction, anti-inflammatory and osteogenesis for facilitating osteointegration and bone regeneration. *Mater Today Bio*. 2025;31:101533.

   doi: 10.1016/j.mtbio.2025.101533

10. Xulin H, Hu L, Liang Q, *et al*. 369Fabrication of 3D gel-printed β-tricalcium phosphate/titanium dioxide porous scaffolds for cancellous bone tissue engineering. *Int J Bioprint*. 2023;9(2):673.

    doi: 10.18063/ijb.v9i2.673

11. Gu X, Zha Y, Li Y, *et al*. Integrated polycaprolactone microsphere-based scaffolds with biomimetic hierarchy and tunable vascularization for osteochondral repair. *Acta Biomater*. 2022;141:190-197.

    doi: 10.1016/j.actbio.2022.01.021

12. Wubneh A, Tsekoura EK, Ayranci C, Uludağ H. Current state of fabrication technologies and materials for bone tissue engineering. *Acta Biomater*. 2018;80:1-30.

    doi: 10.1016/j.actbio.2018.09.031

13. Kouhi M, Khodaei M, Behrouznejad B, Savabi O, Bodaghi M. Zein/ZnO-Modified 3D-Printed PCL/Sphene Scaffolds with Improved Bacterial Inhibition and Osteoblast Activity

for Bone Regeneration Applications. *ACS Biomater Sci Eng*. 2025;11(5):2898-2909.

doi: 10.1021/acsbiomaterials.4c02193

14. Yang CJ, Huang WK, Lin KP. Three-Dimensional Printing Quality Inspection Based on Transfer Learning with Convolutional Neural Networks. *Sensors*. 2023;23(1):491.

doi: 10.3390/s23010491

15. Ren X, Wei J, Luo X, *et al*. HydrogelFinder: A Foundation Model for Efficient Self-Assembling Peptide Discovery Guided by Non-Peptidal Small Molecules. *Adv Sci*. 2024;11(26):e2400829.

doi: 10.1002/advs.202400829

16. Fielder M, Nair AK. Predicting ultrasound wave stimulated bone growth in bioinspired scaffolds using machine learning. *J Mech Behav Biomed Mater*. 2024;159:106684.

doi: 10.1016/j.jmbbm.2024.106684

17. Mohammadrezaei D, Podina L, Silva J, Kohandel M. Cell viability prediction and optimization in extrusion-based bioprinting via neural network-based Bayesian optimization models. *Biofabrication*. 2024;16(2).

doi: 10.1088/1758-5090/ad17cf

18. Bracco F, Zanderigo G, Paynabar K, Colosimo BM. Leveraging transfer learning for efficient bioprinting. *Biofabrication*. 2025;17(3).

doi: 10.1088/1758-5090/ade62f

19. Duan Q, Shao H, Luo N, *et al*. 3D-printed artificial bone scaffolds: the design of materials, the incorporation of bioactive substances, and the integration of vascularized tissue flaps. *Front Bioeng Biotechnol*. 2025;13:1614727.

doi: 10.3389/fbioe.2025.1614727

20. Liu W, Zhang Y, Lyu Y, Bosiakov S, Liu Y. Inverse design of anisotropic bone scaffold based on machine learning and regenerative genetic algorithm. *Front Bioeng Biotechnol*. 2023;11:1241151.

doi: 10.3389/fbioe.2023.1241151

21. Chung JK, Im JS, Park MS. Development of Photo-Polymerization-Type 3D Printer for High-Viscosity Ceramic Resin Using CNN-Based Surface Defect Detection. *Materials*. 2023;16(13):4734.

doi: 10.3390/ma16134734

22. Zhou L, Gjvm VO, Malda J, *et al*. Innovative Tissue-Engineered Strategies for Osteochondral Defect Repair and Regeneration: Current Progress and Challenges. *Adv Healthc Mater*. 2020;9(23):e2001008.

doi: 10.1002/adhm.202001008

23. Semitela A, Marques PAAP, Completo A. Strategies to engineer articular cartilage with biomimetic zonal features: a review. *Biomater Sci*. 2024;12(23):5961-6005.

doi: 10.1039/d4bm00579a

24. Ligon SC, Liska R, Stampfl J, Gurr M, Mülhaupt R. Polymers for 3D Printing and Customized Additive Manufacturing. *Chem Rev*. 2017;117(15):10212-10290.

doi: 10.1021/acs.chemrev.7b00074

25. Xia J, Yuan Y, Wu H, Huang Y, Weitz DA. Decoupling the effects of nanopore size and surface roughness on the attachment, spreading and differentiation of bone marrow-derived stem cells. *Biomaterials*. 2020;248:120014.

doi: 10.1016/j.biomaterials.2020.120014

26. Yang Y, Xu T, Bei HP, *et al*. Gaussian curvature-driven direction of cell fate toward osteogenesis with triply periodic minimal surface scaffolds. *Proc Natl Acad Sci USA*. 2022;119(41):e2206684119.

doi: 10.1073/pnas.2206684119

27. Chen H, Jiang N, Zhang J, *et al*. Micron/Submicron Scaled Hierarchical Ti Phosphate/Ti Oxide Hybrid Coating on 3D Printed Scaffolds for Improved Osteointegration. *ACS Biomater Sci Eng*. 2023;9(3):1274-1284.

doi: 10.1021/acsbiomaterials.2c01354

28. Gehrke SA, da Costa EM, Júnior JA, Eilers Treichel TL, Del Fabbro M, Scarano A. Comparison Between Micro- and Micro-Nano Surface Texturization in the Initial Osseointegration Process: An Experimental In Vitro and In Vivo Preclinical Study. *Bioengineering*. 2025;12(2):175.

doi: 10.3390/bioengineering12020175

29. Critchley S, Sheehy EJ, Cunniffe G, *et al*. 3D printing of fibre-reinforced cartilaginous templates for the regeneration of osteochondral defects. *Acta Biomater*. 2020;113:130-143.

doi: 10.1016/j.actbio.2020.05.040

30. Wu X, Liu S, Chen K, *et al*. 3D printed chitosan-gelatine hydrogel coating on titanium alloy surface as biological fixation interface of artificial joint prosthesis. *Int J Biol Macromol*. 2021;182:669-679.

doi: 10.1016/j.ijbiomac.2021.04.046

31. Tan L, Ye Z, Zhuang W, *et al*. 3D printed PLGA/MgO/PDA composite scaffold by low-temperature deposition manufacturing for bone tissue engineering applications. *Regen Ther*. 2023;24:617-629.

doi: 10.1016/j.reth.2023.09.015

32. Zhang Y, Han Y, Peng Y, Lei J, Chang F. Bionic biphasic composite scaffolds with osteochondrogenic factors for regeneration of full-thickness osteochondral defects. *Biomater Sci*. 2022;10(7):1713-1723.

doi: 10.1039/d2bm00103a

33. Freeman FE, Pitacco P, van Dommelen LHA, *et al*. 3D bioprinting spatiotemporally defined patterns of growth factors to tightly control tissue regeneration. *Sci Adv*.

2020;6(33):eabb5093.

doi: 10.1126/sciadv.abb5093

34. Wang P, Berry D, Moran A, *et al*. Controlled Growth Factor Release in 3D-Printed Hydrogels. *Adv Healthc Mater*. 2020;9(15):e1900977.

doi: 10.1002/adhm.201900977

35. Hunziker EB, Quinn TM, Häuselmann HJ. Quantitative structural organization of normal adult human articular cartilage. *Osteoarthritis Cartilage*. 2002;10(7):564-572.

doi: 10.1053/joca.2002.0814

36. Antons J, Marascio MGM, Nohava J, *et al*. Zone-dependent mechanical properties of human articular cartilage obtained by indentation measurements. *J Mater Sci Mater Med*. 2018;29(5):57.

doi: 10.1007/s10856-018-6066-0

37. Dennis JE, Whitney GA, Rai J, Fernandes RJ, Kean TJ. Physioxia Stimulates Extracellular Matrix Deposition and Increases Mechanical Properties of Human Chondrocyte-Derived Tissue-Engineered Cartilage. *Front Bioeng Biotechnol*. 2020;8:590743.

doi: 10.3389/fbioe.2020.590743

38. Motavalli M, Akkus O, Mansour JM. Depth-dependent shear behavior of bovine articular cartilage: relationship to structure. *J Anat*. 2014;225(5):519-526.

doi: 10.1111/joa.12230

39. Yu X, Hu Y, Zou L, *et al*. A bilayered scaffold with segregated hydrophilicity-hydrophobicity enables reconstruction of goat hierarchical temporomandibular joint condyle cartilage. *Acta Biomater*. 2021;121:288-302.

doi: 10.1016/j.actbio.2020.11.031

40. Camarero-Espinosa S, Rothen-Rutishauser B, Foster EJ, Weder C. Articular cartilage: from formation to tissue engineering. *Biomater Sci*. 2016;4(5):734-767.

doi: 10.1039/c6bm00068a

41. Lei X, Wang X, Li Y, *et al*. Comparison of knee joint and temporomandibular joint development in pig embryos. *Anim Biotechnol*. 2024;35(1):2337760.

doi: 10.1080/10495398.2024.2337760

42. Kupratis ME, Rahman A, Burris DL, Corbin EA, Price C. Enzymatic digestion does not compromise sliding-mediated cartilage lubrication. *Acta Biomater*. 2024;178:196-207.

doi: 10.1016/j.actbio.2024.02.040

43. Lin W, Klein J. Recent Progress in Cartilage Lubrication. *Adv Mater*. 2021;33(18):e2005513.

doi: 10.1002/adma.202005513

44. Forster H, Fisher J. The influence of loading time and lubricant on the friction of articular cartilage. *Proc Inst Mech Eng H*. 1996;210(2):109-119.

doi: 10.1243/PIME_PROC_1996_210_399_02

45. Pouran B, Raoof A, de Winter DAM, *et al*. Topographic features of nano-pores within the osteochondral interface and their effects on transport properties -a 3D imaging and modeling study. *J Biomech*. 2021;123:110504.

doi: 10.1016/j.jbiomech.2021.110504

46. Ruggiero L, Zimmerman BK, Park M, *et al*. Roles of the Fibrous Superficial Zone in the Mechanical Behavior of TMJ Condylar Cartilage. *Ann Biomed Eng*. 2015;43(11):2652-2662.

doi: 10.1007/s10439-015-1320-9

47. Buckley MR, Gleghorn JP, Bonassar LJ, Cohen I. Mapping the depth dependence of shear properties in articular cartilage. *J Biomech*. 2008;41(11):2430-2437.

doi: 10.1016/j.jbiomech.2008.05.021

48. Barthold JE, McCreery KP, Martinez J, *et al*. Particulate ECM biomaterial ink is 3D printed and naturally crosslinked to form structurally-layered and lubricated cartilage tissue mimics. *Biofabrication*. 2022;14(2):025021.

doi: 10.1088/1758-5090/ac584c

49. Zubillaga V, Alonso-Varona A, Fernandes SCM, Salaberria AM, Palomares T. Adipose-Derived Mesenchymal Stem Cell Chondrospheroids Cultured in Hypoxia and a 3D Porous Chitosan/Chitin Nanocrystal Scaffold as a Platform for Cartilage Tissue Engineering. *Int J Mol Sci*. 2020;21(3):1004.

doi: 10.3390/ijms21031004

50. Theodoridis K, Aggelidou E, Manthou ME, Kritis A. Hypoxia Promotes Cartilage Regeneration in Cell-Seeded 3D-Printed Bioscaffolds Cultured with a Bespoke 3D Culture Device. *Int J Mol Sci*. 2023;24(7):6040.

doi: 10.3390/ijms24076040

51. Jiang N, Su Z, Sun Y, *et al*. Spatial Heterogeneity Directs Energy Dissipation in Condylar Fibrocartilage. *Small*. 2023;19(37):e2301051.

doi: 10.1002/smll.202301051

52. Stocum DL, Roberts WE. Part I: Development and Physiology of the Temporomandibular Joint. *Curr Osteoporos Rep*. 2018;16(4):360-368.

doi: 10.1007/s11914-018-0447-7

53. Daly AC, Critchley SE, Rencsok EM, Kelly DJ. A comparison of different bioinks for 3D bioprinting of fibrocartilage and hyaline cartilage. *Biofabrication*. 2016;8(4):045002.

doi: 10.1088/1758-5090/8/4/045002

54. Gologorsky CJ, Middendorf JM, Cohen I, Bonassar LJ. Depth-dependent patterns in shear modulus of temporomandibular joint cartilage correspond to tissue structure and anatomic location. *J Biomech*. 2021;129:110815.

doi: 10.1016/j.jbiomech.2021.110815

55. Hu S, Yi Y, Ye C, Liu J, Wang J. Advances in 3D printing techniques for cartilage regeneration of temporomandibular joint disc and mandibular condyle. *Int J Bioprint*. 2023;9(5):761.

doi: 10.18063/ijb.761

56. Wang X, Wang J, Zhang Y, He Y, Chen S. Piezo1 regulates fibrocartilage stem cell in cartilage growth and osteoarthritis. *Osteoarthritis Cartilage*. 2025;33(8):980-991.

doi: 10.1016/j.joca.2025.04.013

57. Zhao Y, Xie L. An Update on Mesenchymal Stem Cell-Centered Therapies in Temporomandibular Joint Osteoarthritis. *Stem Cells Int*. 2021;2021:6619527.

doi: 10.1155/2021/6619527

58. Su FY, Pang S, Ling YTT, *et al*. Deproteinization of Cortical Bone: Effects of Different Treatments. *Calcif Tissue Int*. 2018;103(5):554-566.

doi: 10.1007/s00223-018-0453-x

59. Beverly M, Marks BE, Murray DW. Subchondral pressures and perfusion during weight bearing. *J Orthop Surg Res*. 2020;15(1):239.

doi: 10.1186/s13018-020-01754-y

60. Chen H, Liu Y, Wang C, *et al*. Design and properties of biomimetic irregular scaffolds for bone tissue engineering. *Comput Biol Med*. 2021;130:104241.

doi: 10.1016/j.compbiomed.2021.104241

61. Jiao J, Hong Q, Zhang D, *et al*. Influence of porosity on osteogenesis, bone growth and osteointegration in trabecular tantalum scaffolds fabricated by additive manufacturing. *Front Bioeng Biotechnol*. 2023;11:1117954.

doi: 10.3389/fbioe.2023.1117954

62. Cheng A, Humayun A, Cohen DJ, Boyan BD, Schwartz Z. Additively manufactured 3D porous Ti-6Al-4V constructs mimic trabecular bone structure and regulate osteoblast proliferation, differentiation and local factor production in a porosity and surface roughness dependent manner. *Biofabrication*. 2014;6(4):045007.

doi: 10.1088/1758-5082/6/4/045007

63. Kumar S, Tan S, Zheng L, Kochmann DM. Inverse-designed spinodoid metamaterials. *npj Comput Mater*. 2020;6:73.

doi: 10.1038/s41524-020-0341-6

64. Zhang M, Lin R, Wang X, *et al*. 3D printing of Haversian bone-mimicking scaffolds for multicellular delivery in bone regeneration. *Sci Adv*. 2020;6(12):eaaz6725.

doi: 10.1126/sciadv.aaz6725

65. Pathria MN, Chung CB, Resnick DL. Acute and Stress-related Injuries of Bone and Cartilage: Pertinent Anatomy, Basic Biomechanics, and Imaging Perspective. *Radiology*. 2016;280(1):21-38.

doi: 10.1148/radiol.16142305

66. Burke G, Devine DM, Major I. Effect of Stereolithography 3D Printing on the Properties of PEGDMA Hydrogels. *Polymers*. 2020;12(9):2015.

doi: 10.3390/polym12092015

67. Sun T, Huang H, Zhao Y, Li Z, Wang H, Zhou G. Low-Temperature Deposited Amorphous Poly(aryl ether ketone) Hierarchically Porous Scaffolds with Strontium-Doped Mineralized Coating for Bone Defect Repair. *Adv Healthc Mater*. 2024;13(23):e2400927.

doi: 10.1002/adhm.202400927

68. Ghobadi E, Yahay Z, Nouri N, Karamali F, Masaeli E. 3D printing of an anatomically shaped bone model inspired by vascularized tubular bone structure. *Biomater Adv*. 2025;176:214348.

doi: 10.1016/j.bioadv.2025.214348

69. Chen H, Gonnella G, Huang J, Di-Silvio L. Fabrication of 3D Bioprinted Bi-Phasic Scaffold for Bone-Cartilage Interface Regeneration. *Biomimetics*. 2023;8(1):87.

doi: 10.3390/biomimetics8010087

70. Wang L, Chen X, Wang X, Chen H, Yang X, Xiao J. Highly biomimetic three-layer mineralized collagen scaffold featuring a wood-reinforced subchondral bone region for gradient chondrogenic-osteogenic differentiation of bone marrow-derived mesenchymal stem cells. *Int J Biol Macromol*. 2025;320(Pt 1):145754.

doi: 10.1016/j.ijbiomac.2025.145754

71. Zhao Y, Cai Y, Wang W, *et al*. Periosteum-bone inspired hierarchical scaffold with endogenous piezoelectricity for neuro-vascularized bone regeneration. *Bioact Mater*. 2024;44:339-353.

doi: 10.1016/j.bioactmat.2024.10.020

72. Tang J, Liu D. Study on the Shock-Absorption Performance of Isolation Systems in High-Rise Vertically Irregular Double-Story Structures. *Buildings*. 2024; 14(12):3792.

doi: 10.3390/buildings14123792

73. Wu D, Zheng K, Yin W, *et al*. Enhanced osteochondral regeneration with a 3D-Printed biomimetic scaffold featuring a calcified interfacial layer. *Bioact Mater*. 2024;36:317-329.

doi: 10.1016/j.bioactmat.2024.03.004

74. Zhou Y, Lian XJ, Lu Y, *et al*. Harnessing oriented arrangement of collagen fibers by 3D printing for enhancing mechanical and osteogenic properties of mineralized collagen scaffolds. *Biomed Mater*. 2024;19(4):045020.

doi: 10.1088/1748-605X/ad5244

75. Burdis R, Chariyev-Prinz F, Kelly DJ. Bioprinting of biomimetic self-organised cartilage with a supporting joint

fixation device. *Biofabrication*. 2021;14(1):015008.

doi: 10.1088/1758-5090/ac36be

76. Wang Z, Tuerxun P, Ng T, *et al*. Enhancing angiogenesis in peri-implant soft tissue with bioactive silk fibroin microgroove coatings on zirconia surfaces. *Regen Biomater*. 2024;11:rbae068.

doi: 10.1093/rb/rbae068

77. Bedell ML, Torres AL, Hogan KJ, *et al*. Human gelatin-based composite hydrogels for osteochondral tissue engineering and their adaptation into bioinks for extrusion, inkjet, and digital light processing bioprinting. *Biofabrication*. 2022;14(4):045012.

doi: 10.1088/1758-5090/ac8768

78. Zub K, Hoeppener S, Schubert US. Inkjet Printing and 3D Printing Strategies for Biosensing, Analytical, and Diagnostic Applications. *Adv Mater*. 2022;34(31):e2105015.

doi: 10.1002/adma.202105015

79. Xie M, Gao Q, Zhao H, *et al*. Electro-Assisted Bioprinting of Low-Concentration GelMA Microdroplets. *Small*. 2019;15(4):e1804216.

doi: 10.1002/smll.201804216

80. Li K, Zhang F, Wang D, *et al*. Silkworm-inspired electrohydrodynamic jet 3D printing of composite scaffold with ordered cell scale fibers for bone tissue engineering. *Int J Biol Macromol*. 2021;172:124-132.

doi: 10.1016/j.ijbiomac.2021.01.013

81. Michailidou G, Terzopoulou Z, Kehagia A, Michopoulou A, Bikiaris DN. Preliminary Evaluation of 3D Printed Chitosan/Pectin Constructs for Biomedical Applications. *Mar Drugs*. 2021;19(1):36.

doi: 10.3390/md19010036

82. Lee J, Oh SJ, An SH, Kim WD, Kim SH. Machine learning-based design strategy for 3D printable bioink: elastic modulus and yield stress determine printability. *Biofabrication*. 2020;12(3):035018.

doi: 10.1088/1758-5090/ab8707

83. Putra NE, Leeflang MA, Klimopoulou M, *et al*. Extrusion-based 3D printing of biodegradable, osteogenic, paramagnetic, and porous FeMn-akermanite bone substitutes. *Acta Biomater*. 2023;162:182-198.

doi: 10.1016/j.actbio.2023.03.033

84. Salehi S, Ghomi H, Hassanzadeh-Tabrizi SA, Koupaei N, Khodaei M. Antibacterial and osteogenic properties of chitosan-polyethylene glycol nanofibre-coated 3D printed scaffold with vancomycin and insulin-like growth factor-1 release for bone repair. *Int J Biol Macromol*. 2025;298:139883.

doi: 10.1016/j.ijbiomac.2025.139883

85. Kuss MA, Wu S, Wang Y, *et al*. Prevascularization of 3D printed bone scaffolds by bioactive hydrogels and cell co-culture. *J Biomed Mater Res B Appl Biomater*. 2018;106(5):1788-1798.

doi: 10.1002/jbm.b.33994

86. Xiong Z, Yan Y, Wang S, Zhang R, Zhang C. Fabrication of porous scaffolds for bone tissue engineering via low-temperature deposition. *Scripta Materialia*. 2002;46(11):771-776.

doi: 10.1016/S1359-6462(02)00071-4.

87. Li Q, Xu S, Feng Q, *et al*. 3D printed silk-gelatin hydrogel scaffold with different porous structure and cell seeding strategy for cartilage regeneration. *Bioact Mater*. 2021;6(10):3396-3410.

doi: 10.1016/j.bioactmat.2021.03.013

88. Liu W, Wang D, Huang J, *et al*. Low-temperature deposition manufacturing: A novel and promising rapid prototyping technology for the fabrication of tissue-engineered scaffold. *Mater Sci Eng C Mater Biol Appl*. 2017;70(Pt 2):976-982.

doi: 10.1016/j.msec.2016.04.014

89. Luo Y, Pan H, Jiang J, *et al*. Desktop-Stereolithography 3D Printing of a Polyporous Extracellular Matrix Bioink for Bone Defect Regeneration. *Front Bioeng Biotechnol*. 2020;8:589094.

doi: 10.3389/fbioe.2020.589094

90. Wang Z, Huang C, Wang J, *et al*. Design and characterization of hydroxyapatite scaffolds fabricated by stereolithography for bone tissue engineering application. *Procedia CIRP*. 2020;89:170-175.

doi: 10.1016/j.procir.2020.05.138

91. Eckstein KN, Hergert JE, Uzcategui AC, *et al*. Controlled Mechanical Property Gradients Within a Digital Light Processing Printed Hydrogel-Composite Osteochondral Scaffold. *Ann Biomed Eng*. 2024;52(8):2162-2177.

doi: 10.1007/s10439-024-03516-x

92. Dobos A, Van Hoorick J, Steiger W, *et al*. Thiol-Gelatin-Norbornene Bioink for Laser-Based High-Definition Bioprinting. *Adv Healthc Mater*. 2020;9(15):e1900752.

doi: 10.1002/adhm.201900752

93. Chen Z, Li K, Han P, *et al*. Stereolithography 3D printing gyroid triply periodic minimal surface vitrified bond diamond grinding wheel. *Sci Rep*. 2024;14(1):30054.

doi: 10.1038/s41598-024-81641-2

94. Shuai C, Li D, Xie H, Yao X, Peng S, Gao C. Programmable Lamellar Eutectic Zn-2Al-Mg Biodegradable Implants Manufactured by Laser Powder Bed Fusion for Synergistic Strength-Ductility and Osteogenesis. *Adv Healthc Mater*. 2025.

doi: 10.1002/adhm.202501917

95. Kérourédan O, Washio A, Handschin C, *et al*. Bioactive gelatin-sheets as novel biopapers to support prevascularization organized by laser-assisted bioprinting for bone tissue engineering. *Biomed Mater*. 2024;19(2):025038.

doi: 10.1088/1748-605X/ad270a

96. Chen Z, Yan X, Yin S, *et al*. Influence of the pore size and porosity of selective laser melted Ti6Al4V ELI porous scaffold on cell proliferation, osteogenesis and bone ingrowth. *Mater Sci Eng C Mater Biol Appl*. 2020;106:110289.

doi: 10.1016/j.msec.2019.110289

97. Yuan X, Zhu W, Yang Z, *et al*. Recent Advances in 3D Printing of Smart Scaffolds for Bone Tissue Engineering and Regeneration. *Adv Mater*. 2024;36(34):e2403641.

doi: 10.1002/adma.202403641

98. Grant-Jacob JA, Zervas MN, Mills B. Laser induced forward transfer imaging using deep learning. *Discov Appl Sci*. 2025;7(4):254.

doi: 10.1007/s42452-025-06679-x

99. Zheng Z, Yu D, Wang H, *et al*. Advancement of 3D biofabrication in repairing and regeneration of cartilage defects. *Biofabrication*. 2025;17(2):022003.

doi: 10.1088/1758-5090/ada8e1

100. Hall GN, Fan Y, Viellerobe B, *et al*. Laser-assisted bioprinting of targeted cartilaginous spheroids for high density bottom-up tissue engineering. *Biofabrication*. 2024;16(4):045029.

doi: 10.1088/1758-5090/ad6e1a

101. Qian Y, Gu Y, Tribukait-Riemenschneider F, Martin I, Shastri VP. Incorporation of Cross-Linked Gelatin Microparticles To Enhance Cell Attachment and Chondrogenesis in Carboxylated Agarose Bioinks for Cartilage Engineering. *ACS Appl Mater Interfaces*. 2025;17(15):22293-22307.

doi: 10.1021/acsami.5c00077

102. Feng C, Zhang W, Deng C, *et al*. 3D Printing of Lotus Root-Like Biomimetic Materials for Cell Delivery and Tissue Regeneration. *Adv Sci (Weinh)*. 2017;4(12):1700401.

doi: 10.1002/advs.201700401

103. Wu Z, Li Z, Wu Y, Hong Y. The Loading of Dipyridamole and Calcium Sulfate into the Gelatin-Coated Porous Bioceramics to Synergistically Regulate Segmental Bone Regeneration. *ACS Appl Mater Interfaces*. 2025;17(43):59108-59123.

doi: 10.1021/acsami.5c14640

104. Jiang Y, Zhou C, Yang X, Ke D. 3D printed bioactive coated scaffolds boost osteogenesis and angiogenesis via the regulation of scaffold microstructure. *Biofabrication*. 2025;17(3):035017.

doi: 10.1088/1758-5090/addc9c

105. Buckley C, Wang H, O'Dell R, *et al*. Creation of Porous, Perfusable Microtubular Networks for Improved Cell Viability in Volumetric Hydrogels. *ACS Appl Mater Interfaces*. 2024;16(15):18522-18533.

doi: 10.1021/acsami.4c00716

106. Li D, Luo F, Yang Y, *et al*. Molten stringing 3D printed microfibrous net-integrated mineralized hydrogels with tunable micromechanical and cell-responsive properties. *J Mater Chem B*. 2025;13(31):9536-9549.

doi: 10.1039/d5tb00449g

107. Feng X, Xu P, Shen T, Zhang Y, Ye J, Gao C. Influence of pore architectures of silk fibroin/collagen composite scaffolds on the regeneration of osteochondral defects in vivo. *J Mater Chem B*. 2020;8(3):391-405.

doi: 10.1039/c9tb01558b

108. Kim MJ, Lee B, Yang K, *et al*. BMP-2 peptide-functionalized nanopatterned substrates for enhanced osteogenic differentiation of human mesenchymal stem cells. *Biomaterials*. 2013;34(30):7236-7246.

doi: 10.1016/j.biomaterials.2013.06.019

109. He L, Zhao M, Cheung JPY, Zhang T, Ren X. Gaussian random field-based characterization and reconstruction of cancellous bone microstructure considering the constraint of correlation structure. *J Mech Behav Biomed Mater*. 2024;152:106443.

doi: 10.1016/j.jmbbm.2024.106443

110. Takagishi T, Yoshioka H, Mikami Y, Oki Y. On-demand inkjet-printed microdisk laser with air cladding by liquid flow microetching. *Appl Opt*. 2020;59(21):6340-6346.

doi: 10.1364/AO.396061

111. Mushtaq RT, Rehman M, Bao C, *et al*. Enhanced biomechanical compatibility of 3D-printed polylactic acid lattice structures: Synergizing mechanical, topography, and microstructural properties for trabecular bone mimicry. *Int J Biol Macromol*. 2025;317(Pt 2):144373.

doi: 10.1016/j.ijbiomac.2025.144373

112. Enriquez-Ochoa D, Robles-Ovalle P, Mayolo-Deloisa K, Brunck MEG. Immobilization of Growth Factors for Cell Therapy Manufacturing. *Front Bioeng Biotechnol*. 2020;8:620.

doi: 10.3389/fbioe.2020.00620

113. Alarcin E, Akguner ZP, Ozturk AB, *et al*. Biomimetic 3D bioprinted bilayer GelMA scaffolds for the delivery of BMP-2 and VEGF exogenous growth factors to promote vascularized bone regeneration in a calvarial defect model in vivo. *Int J Biol Macromol*. 2025;306(Pt 2):141440.

doi: 10.1016/j.ijbiomac.2025.141440

114. He W, Li C, Zhao S, *et al*. Integrating coaxial electrospinning and 3D printing technologies for the development of biphasic porous scaffolds enabling spatiotemporal control in tumor ablation and osteochondral regeneration. *Bioact*

Mater. 2024;34:338-353.

doi: 10.1016/j.bioactmat.2023.12.020

115. Loxley GA, Coser C, Ghaemmaghami AM, Yang J. Long-term interleukin-4 release from 3D printable affinity hydrogels promotes M2-like macrophage polarisation in vitro. *Biomater Sci*. 2025;13(9):2489-2502.

doi: 10.1039/d4bm01623h

116. Wei P, Ma Y, Qin K, Fan Z. A 3D printed biomimetic scaffold for cartilage regeneration with lubrication, load-bearing, and adhesive fixation properties. *Tribol Int*. 2024;192:109328.

doi: 10.1016/j.triboint.2024.109328

117. Ngadimin KD, Stokes A, Gentile P, Ferreira AM. Biomimetic hydrogels designed for cartilage tissue engineering. *Biomater Sci*. 2021;9(12):4246-4259.

doi: 10.1039/d0bm01852j

118. Sasikumar SC, Goswami U, Raichur AM. Mucin-Based Dual Cross-Linkable IPN Hydrogel Bioink for 3D Bioprinting and Cartilage Tissue Engineering. *ACS Appl Bio Mater*. 2025;8(2):1186-1200.

doi: 10.1021/acsabm.4c01505

119. Wu M, Liu H, Zhu Y, *et al*. Bioinspired soft-hard combined system with mild photothermal therapeutic activity promotes diabetic bone defect healing via synergetic effects of immune activation and angiogenesis. *Theranostics*. 2024;14(10):4014-4057.

doi: 10.7150/thno.97335

120. Yang J, Wang H, Huang W, *et al*. A natural polymer-based hydrogel with shape controllability and high toughness and its application to efficient osteochondral regeneration. *Mater Horiz*. 2023;10(9):3797-3806.

doi: 10.1039/d3mh00544e

121. Gupta S, Sharma A, Vasantha Kumar J, Sharma V, Gupta PK, Verma RS. Meniscal tissue engineering via 3D printed PLA monolith with carbohydrate based self-healing interpenetrating network hydrogel. *Int J Biol Macromol*. 2020;162:1358-1371.

doi: 10.1016/j.ijbiomac.2020.07.238

122. Trachsel L, Johnbosco C, Lang T, Benetti EM, Zenobi-Wong M. Double-Network Hydrogels Including Enzymatically Crosslinked Poly-(2-alkyl-2-oxazoline)s for 3D Bioprinting of Cartilage-Engineering Constructs. *Biomacromolecules*. 2019;20(12):4502-4511.

doi: 10.1021/acs.biomac.9b01266

123. Chen Q, Liu S, Yuan Z, Yang H, Xie R, Ren L. Construction and Tribological Properties of Biomimetic Cartilage-Lubricating Hydrogels. *Gels*. 2022;8(7):415.

doi: 10.3390/gels8070415

124. Ali N, Demott CJ, Dingus OF, Grunlan MA, Dunn AC. Network interactions simultaneously enhance stiffness and lubricity of triple-network hydrogels. *Soft Matter*. 2024;20(44):8783-8792.

doi: 10.1039/d4sm00969j

125. Demott CJ, Jones MR, Chesney CD, Grunlan MA. Adhesive Hydrogel Building Blocks to Reconstruct Complex Cartilage Tissues. *ACS Biomater Sci Eng*. 2023;9(4):1952-1960.

doi: 10.1021/acsbiomaterials.2c01438

126. Xu F, Zhuang C, Yao L, *et al*. High-mobility network hydrogel microsphere system to combat chondrocyte senescence for enhanced cartilage repair and regeneration. *Mater Today Bio*. 2025;34:102138.

doi: 10.1016/j.mtbio.2025.102138

127. Lin W, Kluzek M, Iuster N, *et al*. Cartilage-inspired, lipid-based boundary-lubricated hydrogels. *Science*. 2020;370(6514):335-338.

doi: 10.1126/science.aay8276

128. Li S, Tang L, Pu J, *et al*. Continuous Hyaluronic Acid Supply by a UHMWPE/PEEK Interlocking Scaffold for Metatarsophalangeal Joint Prosthesis Lubricating Applications. *ACS Appl Mater Interfaces*. 2025;17(8):11704-11717.

doi: 10.1021/acsami.4c19390

129. Kaneko D, Tada T, Kurokawa T, Gong J. P, Osada Y. Mechanically Strong Hydrogels with Ultra-Low Frictional Coefficients. *Adv. Mater*. 2005, 17 (5), 535–538.

doi: 10.1002/adma.200400739

130. Milner PE, Parkes M, Puetzer JL, *et al*. A low friction, biphasic and boundary lubricating hydrogel for cartilage replacement. *Acta Biomater*. 2018;65:102-111.

doi: 10.1016/j.actbio.2017.11.002

131. Zhang S, Wang L, Kang Y, Wu J, Zhang Z. Nanomaterial-based reactive oxygen species scavengers for osteoarthritis therapy. *Acta Biomater*. 2023;162:1-19.

doi: 10.1016/j.actbio.2023.03.030

132. Shafiq M, Chen Y, Hashim R, He C, Mo X, Zhou X. Reactive Oxygen Species-Based Biomaterials for Regenerative Medicine and Tissue Engineering Applications. *Front Bioeng Biotechnol*. 2021;9:821288.

doi: 10.3389/fbioe.2021.821288

133. Chen Y, Le Y, Yang J, *et al*. 3D Bioprinted Xanthan Hydrogels with Dual Antioxidant and Chondrogenic Functions for Post-traumatic Cartilage Regeneration. *ACS Biomater Sci Eng*. 2024;10(3):1661-1675.

doi: 10.1021/acsbiomaterials.3c01636

134. Sun X, Xu X, Zhao X, *et al*. Three-Dimensional Bioprinted Scaffolds Loaded with Multifunctional Magnesium-Based Metal-Organic Frameworks Improve the Senescence

Microenvironment Prompting Aged Bone Defect Repair. *ACS Nano*. 2025;19(24):22141-22162.

doi: 10.1021/acsnano.5c03023

135. Wang X, Wu S, Li R, *et al*. ROS-Activated Nanohydrogel Scaffolds with Multi-Factors Controlled Release for Targeted Dual-Lineage Repair of Osteochondral Defects. *Adv Sci*. 2025;12(20):e2412410.

doi: 10.1002/advs.202412410

136. He F, Wu H, He B, Han Z, Chen J, Huang L. Antioxidant hydrogels for the treatment of osteoarthritis: mechanisms and recent advances. *Front Pharmacol*. 2024;15:1488036. Published 2024 Oct 25.

doi: 10.3389/fphar.2024.1488036

137. Kuang Y, Hua B, Ye X, Zhao Y, Yu M, Liu X. Dual-functional ROS-responsive hydrogel alleviates temporomandibular joint osteoarthritis by enhancing cartilage repair and mitigating inflammation. *Mater Today Bio*. 2025;33:102103.

doi: 10.1016/j.mtbio.2025.102103

138. Shi W, Fang F, Kong Y, *et al*. Dynamic hyaluronic acid hydrogel with covalent linked gelatin as an anti-oxidative bioink for cartilage tissue engineering. *Biofabrication*. 2021;14(1):10.1088/1758-5090/ac42de.

doi: 10.1088/1758-5090/ac42d

139. Shu C, Qin C, Chen L, *et al*. Metal-Organic Framework Functionalized Bioceramic Scaffolds with Antioxidative Activity for Enhanced Osteochondral Regeneration. *Adv Sci*. 2023;10(13):e2206875.

doi: 10.1002/advs.202206875

140. Zhu S, Zhou Z, Chen X, *et al*. High mechanical performance and multifunctional degraded fucoidan-derived bioink for 3D bioprinting. *Carbohydr Polym*. 2025;348(Pt A):122805.

doi: 10.1016/j.carbpol.2024.122805

141. Helgeland E, Mohamed-Ahmed S, Shanbhag S, *et al*. 3D printed gelatin-genipin scaffolds for temporomandibular joint cartilage regeneration. *Biomed Phys Eng Express*. 2021;7(5):055025.

doi: 10.1088/2057-1976/ac1e68

142. Kalpakci KN, Kim EJ, Athanasiou KA. Assessment of growth factor treatment on fibrochondrocyte and chondrocyte co-cultures for TMJ fibrocartilage engineering. *Acta Biomater*. 2011;7(4):1710-1718.

doi: 10.1016/j.actbio.2010.12.015

143. Yu X, Hu Y, Zou L, *et al*. A bilayered scaffold with segregated hydrophilicity-hydrophobicity enables reconstruction of goat hierarchical temporomandibular joint condyle cartilage. *Acta Biomater*. 2021;121:288-302.

doi: 10.1016/j.actbio.2020.11.031

144. Dufour A, Essayan L, Kim B, Salles V, Marquette C. Biofabrication of Spatially Organized Temporomandibular Fibrocartilage Assembloids. *Adv Healthc Mater*. 2025;14(15):e2405000.

doi: 10.1002/adhm.202405000

145. Jeong HJ, Koch A, Park S, Tarafder S, Lee CH. Bioactive scaffolds integrated with micro-precise spatiotemporal delivery and in vivo degradation tracking for complex tissue regeneration. *Eng Regen*. 2025;6:34-44.

doi: 10.1016/j.engreg.2025.01.001

146. Yi P, Liang J, Huang F, *et al*. Composite system of 3D-printed polymer and acellular matrix hydrogel to repair temporomandibular joint disc. *Front Mater*. 2021;8:621416.

doi: 10.3389/fmats.2021.621416

147. Yu Z, Xing F, Li J, *et al*. 3D printed polycaprolactone/phosphoester-modified poly(amino acid)-graphene oxide scaffold for meniscal regeneration. *J Mater Chem B*. 2025;13(35):11055-11074.

doi: 10.1039/d5tb00012b

148. Trindade D, Alves N, Moura C. From Animal to Human: (Re)using Acellular Extracellular Matrices for Temporomandibular Disc Substitution. *J Funct Biomater*. 2022;13(2):61.

doi: 10.3390/jfb13020061

149. Jiang N, Chen H, Zhang J, *et al*. Decellularized-disc based allograft and xenograft prosthesis for the long-term precise reconstruction of temporomandibular joint disc. *Acta Biomater*. 2023;159:173-187.

doi: 10.1016/j.actbio.2023.01.042

150. Zhang J, Xie L, She Y, Luo H, Zhu S, Jiang N. Microstructural and Micromechanical Properties of Decellularized Fibrocartilaginous Scaffold. *ACS Biomater Sci Eng*. 2025;11(3):1562-1570.

doi: 10.1021/acsbiomaterials.4c01195

151. Lee CH, Rodeo SA, Fortier LA, Lu C, Erisken C, Mao JJ. Protein-releasing polymeric scaffolds induce fibrochondrocytic differentiation of endogenous cells for knee meniscus regeneration in sheep. *Sci Transl Med*. 2014;6(266):266ra171.

doi: 10.1126/scitranslmed.3009696

152. Shen S, Li Y, Chen M, *et al*. Bionic scaffolds with integrated structural components based on low-temperature deposition manufacturing 3D printing technology for the treatment of meniscus defects. *Bioeng Transl Med*. 2025;10(5):e70022.

doi: 10.1002/btm2.70022

153. Savin G, Caillol S, Bethry A, *et al*. Collagen/polyester-polyurethane porous scaffolds for use in meniscal repair. *Biomater Sci*. 2024;12(11):2960-2977.

doi: 10.1039/d4bm00234b

154. Kremer A, Ribitsch I, Reboredo J, *et al*. Three-Dimensional Coculture of Meniscal Cells and Mesenchymal Stem Cells in Collagen Type I Hydrogel on a Small Intestinal Matrix-A Pilot Study Toward Equine Meniscus Tissue Engineering. *Tissue Eng Part A*. 2017;23(9-10):390-402.

doi: 10.1089/ten.TEA.2016.0317

155. Shen S, Chen M, Gao S, *et al*. 3D da yin zhi bei ju ji nei zhi/I xing jiao yuan zu zhi gong cheng ban yue ban zhi jia ji qi li hua te xing de yan jiu [Study on the preparation of polycaprolactone/type I collagen tissue engineered meniscus scaffold by three-dimensional printing and its physiochemical properties]. *Zhongguo Xiu Fu Chong Jian Wai Ke Za Zhi*. 2018;32(9):1205-1210. [In Chinese].

doi: 10.7507/1002-1892.201803074

156. Yao K, Guo K, Wang H, Zheng X. Multi-Nozzles 3D Bioprinting Collagen/Thermoplastic Elasto-Mer Scaffold with Interconnect Pores. *Micromachines*. 2025;16(4):429.

doi: 10.3390/mi16040429

157. Gupta T, Rath P, Pakharenko V, *et al*. Bioinspired thermoreversible bioink orchestrates focal adhesion-dependent osteogenesis. *Trends Biotechnol*. 2026;44(1):239-265.

doi: 10.1016/j.tibtech.2025.09.007

158. Liang R, Li R, Mo W, *et al*. Engineering biomimetic silk fibroin hydrogel scaffolds with "organic-inorganic assembly" strategy for rapid bone regeneration. *Bioact Mater*. 2024;40:541-556.

doi: 10.1016/j.bioactmat.2024.06.024

159. Lu Y, Gong T, Yang Z, Zhu H, Liu Y, Wu C. Designing anisotropic porous bone scaffolds using a self-learning convolutional neural network model. *Front Bioeng Biotechnol*. 2022;10:973275.

doi: 10.3389/fbioe.2022.973275

160. Liang H, Chao L, Xie D, *et al*. Trabecular-like Ti–6Al–4V scaffold for bone repair: A diversified mechanical stimulation environment for bone regeneration. *Compos. Part B Eng.* 2022, 241:110057.

doi: 10.1016/j.compositesb.2022.110057

161. Luo L, Zheng W, Li J, *et al*. 3D-Printed Titanium Trabecular Scaffolds with Sustained Release of Hypoxia-Induced Exosomes for Dual-Mimetic Bone Regeneration. *Adv Sci*. 2025;12(23):e2500599.

doi: 10.1002/advs.202500599

162. Lee SH, Lee J, Kang NU, *et al*. PCL scaffold with well-defined hierarchical pores effectively controls cell migration and alignment of human mesenchymal stem cells. *Sci Rep*. 2025;15(1):11542.

doi: 10.1038/s41598-025-96027-1

163. Tariq S, Shah SA, Hameed F, *et al*. Tissue engineered periosteum: Fabrication of a gelatin basedtrilayer composite scaffold with biomimetic properties for enhanced bone healing. *Int J Biol Macromol*. 2024;263(Pt 2):130371.

doi: 10.1016/j.ijbiomac.2024.130371

164. Feng H, Lian X, Lv S, *et al*. Bioinspired bilayer 3D printing periosteum scaffold with hierarchical structure based on silk fibroin and sodium alginate for bone regeneration. *Int J Biol Macromol*. 2025;310(Pt 2):143175.

doi: 10.1016/j.ijbiomac.2025.143175

165. Chang CH, Lin FH, Lin CC, Chou CH, Liu HC. Cartilage tissue engineering on the surface of a novel gelatin-calcium-phosphate biphasic scaffold in a double-chamber bioreactor. *J Biomed Mater Res B Appl Biomater*. 2004;71(2):313-321.

doi: 10.1002/jbm.b.30090

166. Liu G, Wei X, Zhai Y, *et al*. 3D printed osteochondral scaffolds: design strategies, present applications and future perspectives. *Front Bioeng Biotechnol*. 2024;12:1339916.

doi: 10.3389/fbioe.2024.1339916

167. Bai L, Fang C, Qi Y, Wang C, Wang M. Cryogenic 3D printing of heterogeneous scaffolds with capability to spatially tune cellular morphology of mesenchymal stem cells for integrated osteochondral regeneration. *Mater Today Bio*. 2025;35:102560.

doi: 10.1016/j.mtbio.2025.102560

168. Nowicki MA, Castro NJ, Plesniak MW, Zhang LG. 3D printing of novel osteochondral scaffolds with graded microstructure. *Nanotechnology*. 2016;27(41):414001.

doi: 10.1088/0957-4484/27/41/414001

169. Kotlarz M, O'Keeffe C, S Kronemberger G, *et al*. Biofabrication and in vivo evaluation of a hybrid osteochondral implant consisting of structurally organised engineered cartilage on a 3D-printed metal scaffold. *Biomaterials*. 2026;327:123788.

doi: 10.1016/j.biomaterials.2025.123788

170. Peng Y, Zhuang Y, Liu Y, *et al*. Bioinspired gradient scaffolds for osteochondral tissue engineering. *Exploration*. 2023;3(4):20210043.

doi: 10.1002/EXP.20210043

171. Wang L, Chen X, Wang X, *et al*. Bio-inspired mineralized collagen scaffolds with precisely controlled gradients for the treatment of severe osteoarthritis in a male rabbit model. *Int J Biol Macromol*. 2025;300:139843.

doi: 10.1016/j.ijbiomac.2025.139843

172. Shin J, Kang R, Hyun K, *et al*. Machine Learning-Enhanced Optimization for High-Throughput Precision in Cellular Droplet Bioprinting. *Adv Sci*. 2025;12(20):e2412831.

doi: 10.1002/advs.202412831

173. Yuan B, Guss GM, Wilson AC, *et al*. Machine-Learning-Based Monitoring of Laser Powder Bed Fusion. *Adv Mater*

Technol. 2018;3(12):1800136.

doi: 10.1002/admt.201800136

174. Shin J, Lee Y, Li Z, Hu J, Park SS, Kim K. Optimized 3D Bioprinting Technology Based on Machine Learning: A Review of Recent Trends and Advances. *Micromachines (Basel)*. 2022;13(3):363.

doi:10.3390/mi13030363

175. Jin Z, Zhang Z, Shao X, Gu GX. Monitoring Anomalies in 3D Bioprinting with Deep Neural Networks. *ACS Biomater Sci Eng*. 2023;9(7):3945-3952.

doi: 10.1021/acsbiomaterials.0c0176

176. Shi J, Song J, Song B, Lu WF. Multi-Objective Optimization Design through Machine Learning for Drop-on-Demand Bioprinting. *Engineering*. 2019;5(3):586-593.

doi: 10.1016/j.eng.2018.12.009

177. Li J, Zhou Z, Yang J, *et al*. *MedShapeNet* - a large-scale dataset of 3D medical shapes for computer vision. *Biomed Tech*. 2024;70(1):71-90.

doi: 10.1515/bmt-2024-0396

178. Choi E, An K, Kang KT. Deep-Learning-Based Microfluidic Droplet Classification for Multijet Monitoring. *ACS Appl Mater Interfaces*. 2022;14(13):15576-15586.

doi: 10.1021/acsami.1c22048

179. Jeong JJ, Koo G. AdaLo: Adaptive learning rate optimizer with loss for classification. *Inf Sci*. 2025;690:121607.

doi: 10.1016/j.ins.2024.121607.

180. Chitnis K, Lu Y, Rhoads B, Chakka LRJ, Choudhury S, Maniruzzaman M. Optimization of print parameters for batch and continuous manufacturing of three-dimensional (3D) printed dosage forms using artificial intelligence and machine learning. *Drug Deliv and Transl Res*. 2025.

doi: 10.1007/s13346-025-02006-4

181. Jablonka KM, Patiny L, Smit B. Making the collective knowledge of chemistry open and machine actionable. *Nat Chem*. 2022;14(4):365-376.

doi: 10.1038/s41557-022-00910-7

182. Li F, Han J, Cao T, *et al*. Design of self-assembly dipeptide hydrogels and machine learning via their chemical features. *Proc Natl Acad Sci USA*. 2019;116(23):11259-11264.

doi: 10.1073/pnas.1903376116

183. Javaid S, Gorji HT, Soulami KB, Kaabouch N. Identification and ranking biomaterials for bone scaffolds using machine learning and PROMETHEE. *Res Biomed Eng*. 2023;39:129-138. doi:0.1007/s42600-022-00257-5

184. Nadernezhad A, Groll J. Machine Learning Reveals a General Understanding of Printability in Formulations Based on Rheology Additives. *Adv Sci*. 2022;9(29):e2202638.

doi: 10.1002/advs.202202638

185. Chen H, Liu Y, Balabani S, Hirayama R, Huang J. Machine Learning in Predicting Printable Biomaterial Formulations for Direct Ink Writing. *Research*. 2023;6:0197.

doi: 10.34133/research.0197

186. Yu J, Yao D, Wang L, Xu M. Machine Learning in Predicting and Optimizing Polymer Printability for 3D Bioprinting. Polymers (Basel). 2025;17(13):1873.

doi:10.3390/polym17131873

187. Mai M, Luo S, Fasciano S, *et al*. Morphology-based deep learning approach for predicting adipogenic and osteogenic differentiation of human mesenchymal stem cells (hMSCs). *Front Cell Dev Biol*. 2023;11:1329840.

doi: 10.3389/fcell.2023.1329840

188. Xu H, Liu Q, Casillas J, *et al*. Prediction of cell viability in dynamic optical projection stereolithography-based bioprinting using machine learning. *J Intell Manuf*. 2022;33:995-1005.

doi: 10.1007/s10845-020-01708-5

189. Zhang C., Elvitigala K.C.M.L., Mubarok W., Okano Y., Sakai S. Machine learning-based prediction and optimisation framework for as-extruded cell viability in extrusion-based 3D bioprinting. *Virtual Phys Prototyp*. 2024;19:e2400330.

doi: 10.1080/17452759.2024.2400330

190. Mairpady A, Mourad AI, Mozumder MS. Accelerated Discovery of the Polymer Blends for Cartilage Repair through Data-Mining Tools and Machine-Learning Algorithm. *Polymers*. 2022;14(9):1802.

doi: 10.3390/polym14091802

191. Li Z, Song P, Li G, *et al*. AI energized hydrogel design, optimization and application in biomedicine. *Mater Today Bio*. 2024;25:101014.

doi: 10.1016/j.mtbio.2024.101014

192. Junru Zhang, Yang Liu, Durga Chandra Sekhar.P, *et al*. Rapid, autonomous high-throughput characterization of hydrogel rheological properties via automated sensing and physics-guided machine learning. *Appl. Mater. Today*. 2023;30:14.

doi: 10.1016/j.apmt.2022.101720.

193. Seifermann M, Reiser P, Friederich P, Levkin PA. High-Throughput Synthesis and Machine Learning Assisted Design of Photodegradable Hydrogels. *Small Methods*. 2023;7(9):e2300553.

doi: 10.1002/smtd.202300553

194. Zhao Y, Li H, Zhou H. *et al*. A review of graph neural network applications in mechanics-related domains. *Artif Intell Rev*. 2024;57;315.

doi: 10.1007/s10462-024-10931-y

195. Zahedi S, Taherkhani A, Baserinia R, Zahedi S, Ali, H, Abdi, M. Comparative Evaluation of Neural Networks and Transfer Learning for Predicting Mechanical Properties of 3D-Printed Bone Scaffolds. *Macromol Mater Eng*. 2025; 310.

doi: 10.1002/mame.202500073

196. Shetty A, Fathima A, Anika B, *et al*. Computational optimization of 3D printed bone scaffolds using orthogonal array-driven FEA and neural network modeling. *Sci Rep*. 2025;15(1):30515.

doi: 10.1038/s41598-025-15122-5

197. Wang, Z., Dabaja, R., Chen, L., & Banu, M. Machine learning unifies flexibility and efficiency of spinodal structure generation for stochastic biomaterial design. *Sci Rep*. 2023;13.

doi: 10.1038/s41598-023-31677-7.

198. Ashkan Sedigh, Jacob E. Tulipan, Michael R. Rivlin, Ryan E. Tomlinson. Utilizing Q-Learning to Generate 3D Vascular Networks for Bioprinting Bone. *bioRxiv*. Preprint online 2020.

doi: 10.1101/2020.10.08.331611

199. Cadle R, Rogozea D, Moldovan L, Moldovan NI. Design and Implementation of Anatomically Inspired Mesenteric and Intestinal Vascular Patterns for Personalized 3D Bioprinting. *Appl Sci*. 2022;12(9):4430.

doi: 10.3390/app12094430

200. Wu J, Zhang Y, Lyu Y, Cheng L. On the Various Numerical Techniques for the Optimization of Bone Scaffold. *Materials*. 2023;16(3):974.

doi: 10.3390/ma16030974

201. Drakoulas G, Gortsas T, Polyzos E, Tsinopoulos S, Pyl L, Polyzos D. An explainable machine learning-based probabilistic framework for the design of scaffolds in bone tissue engineering. *Biomech Model Mechanobiol*. 2024;23(3):987-1012.

doi: 10.1007/s10237-024-01817-7

202. Naga Ramesh JV, Sonker A, Indumathi G, Balakrishnan D, Nimma D, Karthik J. Bayesian neural networks for probabilistic modeling of thermal dynamics in multiscale tissue engineering scaffolds. *J Therm Biol*. 2025;130:104134.

doi: 10.1016/j.jtherbio.2025.104134

203. G Taylor S, Mueller E, Jones LR, Makela AV, Ashammakhi N. Translational Aspects of 3D and 4D Printing and Bioprinting. *Adv Healthc Mater*. 2024;13(27):e2400463.

doi: 10.1002/adhm.202400463

204. Seo E, Lee YN, Shin WY, *et al*. Structural influence on titanium ion dissolution in 3D-printed Ti6Al4V orthopedic implants. *Sci Rep*. 2025;15(1):37122.

doi: 10.1038/s41598-025-21129-9

205. Phruekthayanon J, Kühn-Kauffeldt M, Kühn M, *et al*. Biofunctionalization of 3D printed PEEK using integrated cathodic arc plasma coating: a one-step solution to antimicrobial and bioactive PEEK Implant. *J Mater Sci Mater Med*. 2025;36(1):109.

doi: 10.1007/s10856-025-06971-7

206. Grijalva Garces D, Strauß S, Gretzinger S, *et al*. On the reproducibility of extrusion-based bioprinting: round robin study on standardization in the field. *Biofabrication*. 2023;16(1):10.1088/1758-5090/acfe3b.

doi: 10.1088/1758-5090/acfe3b

207. Eraliev O, Lee K-H, Lee C-H. Self-Loosening of a 3D-Printed Bolt by Using Three Different Materials under Cyclical Temperature Changes. *Appl Sci*. 2022; 12(6):3001.

doi: 10.3390/app12063001

208. Mandal A, Clegg JR, Anselmo AC, Mitragotri S. Hydrogels in the clinic. *Bioeng Transl Med*. 2020;5(2):e10158.

doi: 10.1002/btm2.10158

209. Becerra AG, Gutiérrez M, Lahoz-Beltra R. Computing within bacteria: Programming of bacterial behavior by means of a plasmid encoding a perceptron neural network. *Biosystems*. 2022;213:104608.

doi: 10.1016/j.biosystems.2022.104608

210. Sujeeun LY, Phul IC, Goonoo N, Kotov NA, Bhaw-Luximon A. Predicting inflammatory response of biomimetic nanofibre scaffolds for tissue regeneration using machine learning and graph theory. *J Mater Chem B*. 2025;13(10):3304-3318.

doi: 10.1039/d4tb02494j

211. El Arab RA, Al Moosa OA, Sagbakken M. Economic, ethical, and regulatory dimensions of artificial intelligence in healthcare: an integrative review. *Front Public Health*. 2025;13:1617138.

doi: 10.3389/fpubh.2025.1617138

212. Silva Robazzi JV, Derman ID, Gupta D, *et al*. The Synergy of Artificial Intelligence and 3D Bioprinting: Unlocking New Frontiers in Precision and Tissue Fabrication. *Adv Funct Mater*. 2025.

doi: 10.1002/adfm.202509530